EAI-TR-79-004

ATMOSPHERIC TURBULENCE SIMULATION

FOR

SHUTTLE ORBITER

Summary Report
Contract NAS8-33076

Prepared For:

National Aeronautics and Space Administration
George C. Marshall Space Flight Center
Marshall Space Flight Center, Alabama 35812

Prepared By:

Frank B. Tatom
S. Ray Smith

August 31, 1979

ENGINEERING ANALYSIS, INC.

2109 Clinton Ave. W., Suite 432
Huntsville, Alabama 35805
(205)533-9391

TABLE OF CONTENTS

LIST OF ILLUSTRATIONS

LIST OF ILLUSTRATIONS
(Continued)

LIST OF SYMBOLS

English Symbols

Symbol	Definition
a	von Karman constant (1.339)
$h(\ell)$	discrete impulse response function
$h(t)$	impulse response function
k	magnitude of wave number vector
k_i	component of wave number vector
K	dimensionless magnitude of wave number vector (aLk)
K_i	dimensionless wave number (aLk_i)
L	characteristic length scale
ℓ_x, ℓ_y, ℓ_z	characteristic dimensions of vehicle
t	dimensionless time ($V\tau/aL$)
T	dimensionless time step ($V\Delta\tau/aL$)
u_i	gust velocity component
V	magnitude of vehicle velocity
x_i	Cartesian coordinate component
$X(n)$	white noise input
$Y_x(n)$	simulated turbulence output based on $X(n)$

Greek Symbols

Symbol	Definition
σ^2	variance
τ	time
$\Phi_{ii}(K_1, K_2, K_3)$	three-dimensional gust spectrum with dimensionless wave numbers
$\Phi_{ii/jj}(K_1, K_2, K_3)$	three-dimensional gust gradient spectrum with dimensionless wave numbers
$\Phi_{ii}(K_1)$	one-dimensional gust spectrum with dimensionless wave numbers

LIST OF SYMBOLS
(continued)

Greek Symbols

Symbol	Definition
$\Phi_{ii/jj}(K_1)$	one-dimensional gust gradient spectrum with dimensionless wave numbers
ω	frequency (kV)
Ω	dimensionless frequency ($aL\omega/V$)

Miscellaneous Symbols

Symbol	Definition
$< >$	ensemble average

1. INTRODUCTION

The effects of atmospheric turbulence in both horizontal and near-horizontal flight, during the return of the Space Shuttle, are important for determining design, control, and "pilot-in-the-loop" effects. An improved non-recursive model for atmospheric turbulence along the flight path of the Shuttle Orbiter has been developed which provides for simulation of instantaneous vertical and horizontal gusts at the vehicle center-of-gravity, and also for simulation of instantaneous gust gradients. Based on this model the time series for both gusts and gust gradients have been generated and stored on a series of magnetic tapes.

Section 2 provides a description of the various technical considerations associated with the turbulence simulation model. Included in this section are descriptions of the digital filter simulation model, the von Karman spectra with finite upper limits, and the final non-recursive turbulence simulation model which was used to generate the time series.

Section 3 provides a description of the time series as currently recorded on magnetic tape. Conclusions and recommendations are presented in Section 4 while references cited are listed in Section 5.

2. TECHNICAL DISCUSSION

Based on earlier efforts [1] an improved turbulence simulation model had been already developed. In the course of the current study this simulation model was subjected to additional analysis and revision in order to produce a more practical simulation tool. The additional analyses and revisions are described in the subsections which follow.

2.1 DIGITAL FILTER SIMULATION

The existing turbulence model, based on digital filter simulation [1], involved the solution of digital filter difference equations which were derived from z-transform theory [2]. The previously developed combined von Karman - Saffman spectra [1] were approximated by means of a series of general meromorphic functions of the form

$$\Phi = \sum_{i=1}^{N}\sum_{\ell=1}^{N} A_i A_\ell \frac{R_{bi}R_{b\ell}R_{di}R_{c\ell}}{R_{ci}R_{c\ell}R^2_{fi}R^2_{f\ell}} \exp\Big[j(\Theta_{bi}-\Theta_{b\ell}+\Theta_{di}-\Theta_{d\ell} -\Theta_{ci}+\Theta_{c\ell}-2\Theta_{fi}+2\Theta_{f\ell})\Big] \tag{1}$$

where

A_n = coefficient (based on curve fit)

$R_{bn} = (b_n^2 + \Omega^2)^{1/2}$

$R_{cn} = (c_n^2 + \Omega^2)^{1/2}$

$R_{dn} = (c_n^2 + \Omega^2)1/2$

$R_{fn} = (f_n^2 + \Omega^2)^{1/2}$

$\Theta_{bn} = \arctan(\Omega/b_n)$

$\Theta_{cn} = \arctan(\Omega/c_n)$

$\Theta_{dn} = \arctan(\Omega/d_n)$

$\Theta_{fn} = \arctan(\Omega/f_n)$

Ω = dimensionless frequency ($aL\omega/V$)

b_n = constant (based on curve fit)

c_n = constant (based on curve fit)

d_n = constant (based on curve fit)

f_n = constant (based on curve fit)

2.1.1 Development of Revised Meromorphic Function

Each term in the preceding general meromorphic function contained five coefficients, A_n, b_n, c_n, d_n, and f_n. The values for these coefficients were obtained by curve-fitting the specific gust or gust-gradient spectrum. For a series approximation involving N terms, values had to be established for a total of 5 N coefficients. Because of the number of coefficients involved, and the nonlinear characteristics of the terms, a numerical method based on the Newton-Raphson method coupled with the Freudenstein-Roth technique [3] was utilized as a means of assigning values to the coefficients. This approach proved only partially successful due to matrix inversion problems. Such problems were caused by the limited number of double-precision significant figures (12 or 13) available on the HP-21MX digital computer. In addition, the selection of initial guesses for the coefficients proved to be difficult because of the relatively complex form of the functions.

For the reasons noted a revised meromorphic function (RMF) with a simpler form was developed as follows:

$$\Phi = \sum_{i=1}^{N} \sum_{k=1}^{N} \frac{A_i A_k \Omega^2}{(R_{fi})^M (R_{fk})^M} \exp[jM(\theta_{fi} - \theta_{fk})] \qquad (2)$$

where

A_n = Coefficient (based on curve fit)

R_{fn} = $(f_n^2 + \Omega^2)^{1/2}$

θ_{fn} = $\arctan(\Omega/f_n)$

f_n = constant (based on curve fit)

M = power coefficient (normally = 2)

Each RMF term contained only two empirical constants to be computed, A_n and f_n. The power coefficient, M, could be assigned any positive integer* value but a value of +2 proved to be generally appropriate.

2.1.2 Development of RMF Difference Equation

Based on the same approach used previously with other meromorphic functions [1], the difference equation based on the RMF was derived as follows:

$$Y_x(k) = \frac{1}{G_{M,0}} \sum_{j=1}^{MN} \left[W_j \, X(k-j) - G_{M,j} \, Y_x(k-j) \right] \tag{3}$$

where

$$G_{m+1,j} = \sum_{\ell=0}^{j} D_\ell \, G_{m,j-\ell}$$

$$G_{0,0} = 1$$

$$G_{m,j} = 0 \quad (j>mN)$$

$$D_\ell = (-1)^\ell \times \text{elementary symmetric function of } C_j (0 \le j \le N)$$

$$C_j = \exp(-f_j T)$$

$$T = \text{dimensionless time step}$$

$$W_j = \frac{T^{M-1} V_j}{(M-1)!}$$

$$V_j = \sum_{i=1}^{N} A_i \, H_{M,j,i}$$

$$H_{M,j,i} = \sum_{\ell=1}^{M} (\beta_\ell C_i^{\ell} - \beta_{\ell-1} C_i^{\ell-1}) \, G_{M,j-\ell,i}$$

*Greater than unity

$$G_{m+1,j,i} = \sum_{\ell=0}^{j} D_{\ell,i}\, G_{m,j-\ell,i}$$

$$G_{0,j,i} = 1$$

$$G_{m,j,i} = 0 \qquad (j>mN-m)$$

$$D_{\ell,i} = (-1)^{\ell} \times \text{elementary symmetric function of } C_j (0 \leq j \leq N), \text{ omitting } C_i$$

2.1.3 Spectral Curve Fits

The RMF was utilized to develop approximations for several different spectra. As before the values of A_i and f_i for each term in the series approximation was computed by means of the Newton-Raphson method coupled with the Freudenstein-Roth technique. In general this curve-fitting procedure proved satisfactory but considerable care was necessary in the selection of the initial guesses in order to achieve convergence. Examples of the spectral curve fits for the combined von Karman - Saffman spectra Φ_{22} and $\Phi_{11/11}$ are provided in Figures 2-1 and 2-2.

2.1.4 Numerical Instability of RMF Difference Equations

The RMF difference equations previously developed were incorporated into a digital computer program suitable for the HP-21MX. The program was subjected to a number of tests to insure that the various intermediate arrays associated with the RMF series were properly computed.

A series of test runs were carried out with a nine-term RMF series approximation of Φ_{22}. In all such test runs the resulting output, representing the y-component of the turbulent gusts, increased until the limit of the computer was reached. This buildup apparently resulted from the large values of $G_{M,j}$ associated with the nine-term RMF series. Several methods were used in an attempt to avoid such a buildup. Variation of the time step, T, had little effect. No amount of scale reduction proved sufficient to avoid the buildup.

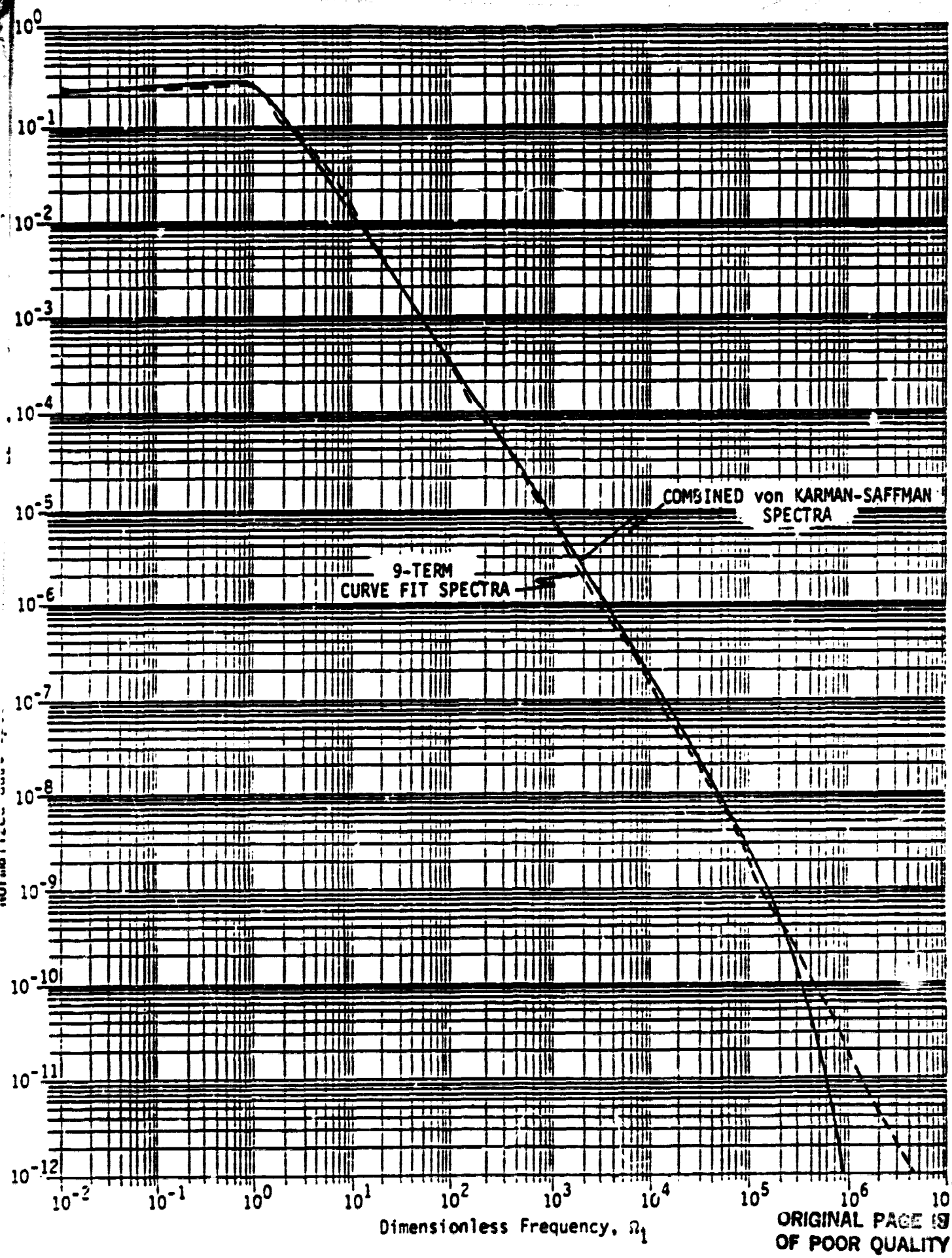

Figure 2-1. Curve Fit (9-term) of Normalized Gust Spectra $\Phi_{22}(\Omega_1)$ or $\Phi_{33}(\Omega_1)$

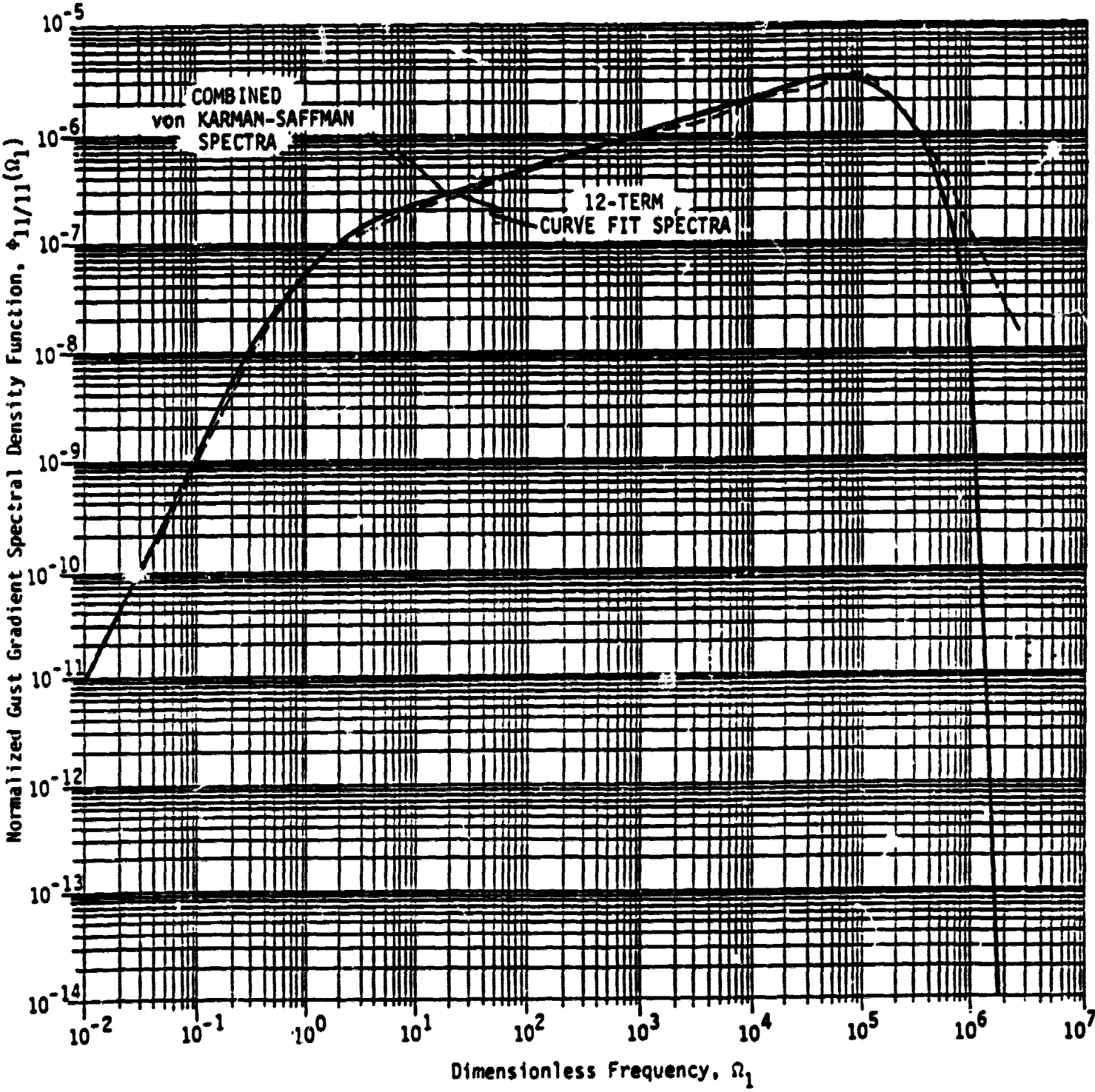

Figure 2-2. Curve Fit (12-term) of Normalized Gust Gradient Spectra $\Phi_{11/11}(\Omega_1)$

Similar problems with instability were apparently encountered initially in earlier work using simpler meromorphic functions [2,4]. In those cases as the computations proceeded, however, the instabilities died out and subsequent output proved stable [5]. For the current case involving a more complex series of meromorphic functions, the instability did not die out in spite of various attemps to scale it down. The conclusion was reached that the basic difference equation was inherently unstable and thus not suitable for use in a turbulence simulation model.

2.2 DEVELOPMENT OF VON KARMAN SPECTRA WITH FINITE UPPER LIMITS

The combined von Karman - Saffman spectra [1] had been used for all work involving the digital filter simulation concept described in subsection 2.1. Based on a further analysis of the ranges of wavenumbers over which the turbulence model was valid [6], the combined von Karman - Saffman spectra integrated over all wavenumbers were replaced by von Karman spectra with finite upper limits of integration. The basic three-dimensional relation to be integrated for the dimensionless gust spectra was [7],

$$\phi_{ii}(K_1,K_2,K_3) = \frac{55\sigma^2}{36a\pi^2} \frac{(K^2-K_i^2)}{(1+K^2)^{17/6}} \tag{4}$$

The corresponding relation for gust gradient spectra was

$$\phi_{ii/jj}(K_1,K_2,K_3) = \left(\frac{\sigma^2}{L^2}\right)\left(\frac{55}{36\pi^2a^3}\right) \frac{K_j^2(K^2-K_i^2)}{(1+K^2)^{17/6}} \tag{5}$$

2.2.1 Upper Limits of Integration

The upper limits of integration were based on three characteristic dimensions of the Space Shuttle [8] as shown in Table 2-1.

TABLE 2-1. CHARACTERISTIC DIMENSIONS OF SPACE SHUTTLE

Characteristic Length	Magnitude (ft)	Explanation
ℓ_x	38.8	mean aerodynamic chord
ℓ_y	39.05	1/2 wingspan
ℓ_z	10.95	1/2 fuselage thickness

The scale of turbulence, L, was taken to be 762 meters or 2500 feet. The maximum dimensionless wavenumbers corresponding to the characteristic dimensions are presented in Table 2-2.

TABLE 2-2. MAXIMUM DIMENSIONLESS WAVENUMBERS

Wavenumber	Definition	Magnitude
K_{1max}	aL/ℓ_x	86.3
K_{2max}	aL/ℓ_y	85.7
K_{3max}	aL/ℓ_z	305.7

2.2.2 One-Dimensional Spectra

Based on second-order numerical integration the preceding gust and gust gradient spectral relations were integrated over K_3 and K_2 (with the appropriate upper limits). The resulting one-dimensional spectra are presented in Appendix A. As indicated in the appendix the spectra were computed for values of Ω_1* in excess of K_{1max}. These computations were necessary because of the need for establishing a Nyquist cutoff frequency

*The dimensionless frequency $\Omega_1 (=aL\omega_1/V)$ is equivalent to the dimensionless wave number $K_1 (=aLk_1)$.

for each spectra, as discussed in the subsection 2.2.3. The spectra have also been normalized based on an upper limit of Ω_1 which equals 100 K_{1max}.

2.2.3 Nyquist Cutoff Frequencies

The finite limit $\Omega_{1max}(=K_{1max})$ previously developed corresponds to the optimum dimensionless sampling frequency. The Nyquist cutoff frequency, Ω_{1N}, however should be greater than this optimum sampling frequency because of the distortion to the spectra due to the finite upper limit [4]. This distortion can be expressed in the form of a modified spectrum $\Phi'(\Omega_1)$ where

$$\Phi'(\Omega_1) = \Phi(\Omega_1) \frac{\sin^2(\pi\Omega_1/\Omega_{1N})}{(\pi\Omega_1/\Omega_{1N})^2} + \Phi(2\Omega_{1max} - \Omega_1) \frac{\sin^2[\pi(2\Omega_{1max} - \Omega_1)/\Omega_{1N}]}{[\pi(2\Omega_{1max} - \Omega_1)/\Omega_{1N}]^2} \quad (6)$$

The value of $\Phi(\Omega_{1N})$ must be selected such that $\Phi'(\Omega_1)$ closely resembles $\Phi(\Omega_1)$ for $\Omega_1 \leq \Omega_{1max}$. A series of test runs were carried out comparing $\Phi'(\Omega_1)$ with $\Phi(\Omega_1)$ for various values of Ω_{1N}.

Based on the series of test runs a Nyquist cutoff frequency, Ω_{1N}, was computed for each spectra as shown in Table 2-3. These cutoff frequencies are also included in Figures A-1 through A-12. The basic criterion for computing the cutoff frequencies was that

$$\int_0^{\Omega_{1max}} \Phi(\Omega_1)d\Omega_1 = \int_0^{\Omega_{1max}} \Phi'(\Omega_1)d\Omega_1 \quad (7)$$

The resulting modified spectra, $\Phi'(\Omega_1)$, produced by such cutoff frequencies generally resemble the original spectra, $\Phi(\Omega_1)$, as indicated in Tables B-1 through B-12 of Appendix B.

TABLE 2-3. NYQUIST CUTOFF FREQUENCIES

Spectra	Dimensionless Nyquist Cutoff Frequency, Ω_{1N}	Ratio*
Φ_{11}	300.0	.9995
Φ_{22}	285.0	1.0006
Φ_{33}	285.0	1.0000
$\Phi_{11/11}$	205.0	1.0008
$\Phi_{11/22}$	260.0	.9939
$\Phi_{11/33}$	225.0	.9959
$\Phi_{22/11}$	193.0	1.0021
$\Phi_{22/22}$	225.0	.9923
$\Phi_{22/33}$	215.0	.9972
$\Phi_{33/11}$	195.0	1.0006
$\Phi_{33/22}$	245.0	1.0004
$\Phi_{33/33}$	210.0	1.0065

$$^{*}\text{Ratio} = \frac{\int_0^{\Omega_{1max}} \Phi'(\Omega_1)\,d\Omega_1}{\int_0^{\Omega_{1max}} \Phi(\Omega_1)\,d\Omega_1}$$

2.2.4 Normalization of Spectra

As noted previously the spectra presented in Figures A-1 through A-12 extend to an upper limit of Ω_1 which equals 100 K_{1max}. Numerical integration of these spectra with respect to Ω_1 was carried out to obtain $\langle u_i u_i' \rangle$ and $\left\langle \frac{\partial u_i}{\partial x_j} \frac{\partial u_i'}{\partial x_j'} \right\rangle$ with the following results:

$$\begin{pmatrix} \langle u_1 u_1' \rangle \\ \langle u_2 u_2' \rangle \\ \langle u_3 u_3' \rangle \end{pmatrix} = \sigma^2 \begin{pmatrix} .9541 \\ .9661 \\ .9556 \end{pmatrix} \qquad \begin{matrix} (K_{1\text{limit}} = 8630, \\ K_{2\text{limit}} = 85.7, \\ K_{3\text{limit}} = 305.7) \end{matrix} \tag{8}$$

and

$$\begin{pmatrix} \left\langle \frac{\partial u_1}{\partial x_1} \frac{\partial u_1'}{\partial x_1'} \right\rangle & \left\langle \frac{\partial u_1}{\partial x_2} \frac{\partial u_1'}{\partial x_2'} \right\rangle & \left\langle \frac{\partial u_1}{\partial x_3} \frac{\partial u_1'}{\partial x_3'} \right\rangle \\ \left\langle \frac{\partial u_2}{\partial x_1} \frac{\partial u_2'}{\partial x_1'} \right\rangle & \left\langle \frac{\partial u_2}{\partial x_2} \frac{\partial u_2'}{\partial x_2'} \right\rangle & \left\langle \frac{\partial u_2}{\partial x_3} \frac{\partial u_2'}{\partial x_3'} \right\rangle \\ \left\langle \frac{\partial u_3}{\partial x_1} \frac{\partial u_3'}{\partial x_1'} \right\rangle & \left\langle \frac{\partial u_3}{\partial x_2} \frac{\partial u_3'}{\partial x_2'} \right\rangle & \left\langle \frac{\partial u_3}{\partial x_3} \frac{\partial u_3'}{\partial x_3'} \right\rangle \end{pmatrix}$$

$$= \frac{\sigma^2}{L^2} \begin{pmatrix} 130.07 & 97.174 & 249.92 \\ 631.76 & 71.368 & 308.62 \\ 574.74 & 98.862 & 128.39 \end{pmatrix} \qquad \begin{matrix} (K_{1\text{limit}} = 8630, \\ K_{2\text{limit}} = 85.7, \\ K_{3\text{limit}} = 305.7) \end{matrix} \tag{9}$$

The right-hand sides of Eqs (8) and (9) represent the normalization constants based on upper limits of 100 K_{1max}, K_{2max}, and K_{3max}. The corresponding normalization constants based on upper limits of Ω_{1N}*, K_{2max}, and K_{3max} were obtained by interpolating the numerical values of cumulative distribution functions which were computed in conjunction with the numerical integration previously noted. The results were as follows:

$$\begin{pmatrix} \langle u_1 u_1' \rangle \\ \langle u_2 u_2' \rangle \\ \langle u_3 u_3' \rangle \end{pmatrix} = \sigma^2 \begin{pmatrix} .9199 \\ .9428 \\ .9231 \end{pmatrix} \qquad \begin{matrix} (K_{1limit} = \Omega_{1N}, \\ K_{2limit} = 85.7, \\ K_{3limit} = 305.7) \end{matrix} \tag{10}$$

$$\begin{pmatrix} \langle \frac{\partial u_1}{\partial x_1} \frac{\partial u_1'}{\partial x_1'} \rangle & \langle \frac{\partial u_1}{\partial x_2} \frac{\partial u_1'}{\partial x_2'} \rangle & \langle \frac{\partial u_1}{\partial x_3} \frac{\partial u_1'}{\partial x_3'} \rangle \\ \langle \frac{\partial u_2}{\partial x_1} \frac{\partial u_2'}{\partial x_1'} \rangle & \langle \frac{\partial u_2}{\partial x_2} \frac{\partial u_2'}{\partial x_2'} \rangle & \langle \frac{\partial u_2}{\partial x_3} \frac{\partial u_2'}{\partial x_3'} \rangle \\ \langle \frac{\partial u_3}{\partial x_1} \frac{\partial u_3'}{\partial x_1'} \rangle & \langle \frac{\partial u_3}{\partial x_2} \frac{\partial u_3'}{\partial x_2'} \rangle & \langle \frac{\partial u_3}{\partial x_3} \frac{\partial u_3'}{\partial x_3'} \rangle \end{pmatrix}$$

$$= \frac{\sigma^2}{L^2} \begin{pmatrix} 79.38 & 94.34 & 226.75 \\ 184.66 & 64.30 & 242.24 \\ 166.21 & 95.60 & 84.78 \end{pmatrix} \qquad \begin{matrix} (K_{1limit} = \Omega_{1N}, \\ K_{2limit} = 85.7, \\ K_{3limit} = 305.7) \end{matrix} \tag{11}$$

*The values of Ω_{1N} vary from spectra to spectra as shown in Table 2-3.

In similar fashion the corresponding normalization constants based on upper limits of K_{1max}, K_{2max}, and K_{3max} were obtained by interpolation with the following results:

$$\begin{pmatrix} \langle u_1 u_1' \rangle \\ \langle u_2 u_2' \rangle \\ \langle u_3 u_3' \rangle \end{pmatrix} = \sigma^2 \begin{pmatrix} .9027 \\ .9143 \\ .8967 \end{pmatrix} \qquad \begin{matrix} (K_{1limit} = 86.3, \\ K_{2limit} = 85.7, \\ K_{3limit} = 305.7) \end{matrix} \qquad (12)$$

$$\begin{pmatrix} \langle \frac{\partial u_1}{\partial x_1} \frac{\partial u_1'}{\partial x_1'} \rangle & \langle \frac{\partial u_1}{\partial x_2} \frac{\partial u_1'}{\partial x_2'} \rangle & \langle \frac{\partial u_1}{\partial x_3} \frac{\partial u_1'}{\partial x_3'} \rangle \\ \langle \frac{\partial u_2}{\partial x_1} \frac{\partial u_2'}{\partial x_1'} \rangle & \langle \frac{\partial u_2}{\partial x_2} \frac{\partial u_2'}{\partial x_2'} \rangle & \langle \frac{\partial u_2}{\partial x_3} \frac{\partial u_2'}{\partial x_3'} \rangle \\ \langle \frac{\partial u_3}{\partial x_1} \frac{\partial u_3'}{\partial x_1'} \rangle & \langle \frac{\partial u_3}{\partial x_2} \frac{\partial u_3'}{\partial x_2'} \rangle & \langle \frac{\partial u_3}{\partial x_3} \frac{\partial u_3'}{\partial x_3'} \rangle \end{pmatrix}$$

$$= \frac{\sigma^2}{L^2} \begin{pmatrix} 55.36 & 88.82 & 190.06 \\ 91.29 & 53.48 & 191.96 \\ 82.71 & 82.08 & 62.09 \end{pmatrix} \qquad \begin{matrix} (K_{1limit} = 86.3, \\ K_{2limit} = 85.7, \\ K_{3limit} = 305.7) \end{matrix} \qquad (13)$$

2.3 NON-RECURSIVE TURBULENCE SIMULATION

The numerical instability associated with the digital filter simulation as described in subsection 2.1.4 was due in part to the recursive nature of the model. In an effort to retain the meromorphic function series approximations of the gust and gust gradient spectra, an alternate set of non-recursive difference equations were derived based on a binominal series expression. The final equation was as follows:

$$Y_x(k) = \frac{T^{M-1}}{(M-1)!} \sum_{j=1}^{J} R_{N,M,j}\, X(k-j) \tag{14}$$

where

T = dimensionless time step (π/Ω_{1N})

M = power coefficient (normally =2)

$$R_{N,M,j} = \sum_{i=1}^{N} A_i \sum_{\ell=1}^{M-1} B_\ell \left[\binom{j+M-1-\ell}{M-1} C_i^{\,j} - \binom{j+M-2-\ell}{M-1} C_i^{\,j-1} \right]$$

A_i = coefficient (based on curve fit)

B_ℓ = z-transform coefficient (depending on M)

C_i = $\exp(-f_i T)$

f_i = constant (based on curve fit)

$\binom{m}{n}$ = binomial coefficient $\left(= \frac{m!}{(m-n)!n!}\right)$

Eq (14) differs from the original RMF difference equation (3) in that the later was recursive while the former is not. Thus Eq (14) is not subject to the type of instability previously encountered with Eq (3).

Although Eq (14) represents a reasonable alternative to the original approach, there exists an easier, more direct method of generating an equivalent non-recursive model. As developed by Perlmutter [9] a simulated turbulent signal can be generated by the relation

$$Y'_x(k) = T \sum_{j=-N}^{+N} h(j)\, X(k-j) \tag{15}$$

where

$Y'_x(k)$ = discrete sampled output based on white noise input $X(k)$

$h(\ell) = h(\ell T)$

$= h(t)$ (the impulse response function)

$X(k)$ = discrete sampled white noise input

To correct for the effect of digitizing, Eq (15) must be divided by $\sqrt{T}$ [10]. Thus,

$$Y_x(k) = Y_x'(k)/\sqrt{T}$$

$$= \sqrt{T} \sum_{j=-N}^{N} h(j)\, X(k-j) \tag{16}$$

Eq (16) represents a relatively simple non-recursive relation for turbulence simulation based on a white noise source and an impulse response function.

The impulse response function is the inverse Fourier tranform of the square root of the one-dimensional spectra. Therefore

$$h(t) = F^{-1}[\Phi(\Omega_1)^{1/2}] \tag{17}$$

Thus

$$h(t) = \frac{1}{2\pi}\int_{-\infty}^{\infty} [\Phi(\Omega_1)]^{1/2} \exp(j\Omega_1 t)\, d\Omega_1$$

$$= \frac{1}{2\pi}\int_{-\infty}^{\infty} [\Phi(\Omega_1)]^{1/2} [\cos(\Omega_1 t) + j \sin(\Omega_1 t)]\, d\Omega_1 \tag{18}$$

Now $\sin(\Omega_1 t)$ is odd while $[\Phi(\Omega_1 t)]^{1/2}$ and $\cos(\Omega_1 t)$ are even. Thus

$$h(t) = \frac{1}{\pi}\int_{0}^{\infty} [\Phi(\Omega_1)]^{1/2} \cos(\Omega_1 t)\, d\Omega_1 \tag{19}$$

By means of second-order numerical integration [11] the discrete inverse Fourier transforms were computed for the square root of the gust and gust gradient spectra, shown in Figures A-1 through A-12. The numerical integration for each spectra was limited to the frequency interval from 0 to Ω_{1N}. The computed transforms are presented in Figures C-1 through C-12 of Appendix C. Based on Eq (16) these transforms were used with a white noise source, RNORM [1], to generate simulated turbulence gusts and gust gradients.

3. TIME SERIES FOR SIMULATED TURBULENCE

The non-recursive turbulence simulation model described in subsection 2.3 has been incorporated into a digital computer program TBSIM. This program is currently operational on the HP-21MX digital computer in the MSFC Space Sciences Laboratory. The inputs to TBSIM are the impulse response function, $h(\ell)$ for each spectrum, and white noise from RNORM [1]. The outputs of TBSIM are the simulated turbulence time series written in dimensionless form and stored on magnetic tapes.

3.1 CHARACTERISTICS OF DIMENSIONLESS TIME SERIES

The sampling interval for each time series corresponds to the *dimensionless* time step T ($=\pi/\Omega_{1N}$). The corresponding *dimensional* time step can be obtained by the relation

$$\Delta\tau = \pi aL/(V\Omega_{1N}) \qquad (20)$$

The value of the Nyquist cutoff frequency Ω_{1N} for each spectrum is provided in Table 2-3. The dimensionless time step and number of time steps for each series are indicated in Table 3-1. The *dimensionless* gust and gust gradients represented by the amplitude of the series can be converted to *dimensional* form by multiplying by the normalization constants presented in Eqs (10) and (11). Portions of the time series for the x_1-gust and the $\frac{\partial u_1}{\partial x_1}$- gust gradient are presented in Figures 3-1 and 3-2 respectively.

3.2 CHARACTERISTICS OF MAGNETIC TAPES

Each of the twelve simulated turbulence time series (corresponding to the three gust spectra and the nine gust gradient spectra) is written on a separate nine-tract magnetic tape as indicated in Table 3-1. Pertinent characteristics of the tapes are summarized in Table 3-2.

The first record on each tape contains a 34-character alphanumeric descriptor. The second record contains the spectrum identification (NINT), the number of points in the time series (MMAX), and the time series step size (T). The format for this record is "2I10,5X,E14.7". Following these two records, the time series is stored on tape as MMAX records. Each such record consists of the time (ST) and the corresponding value of turbulent gust or gust gradient (Y). The format for these records is "E14.7,2X,E14.7".

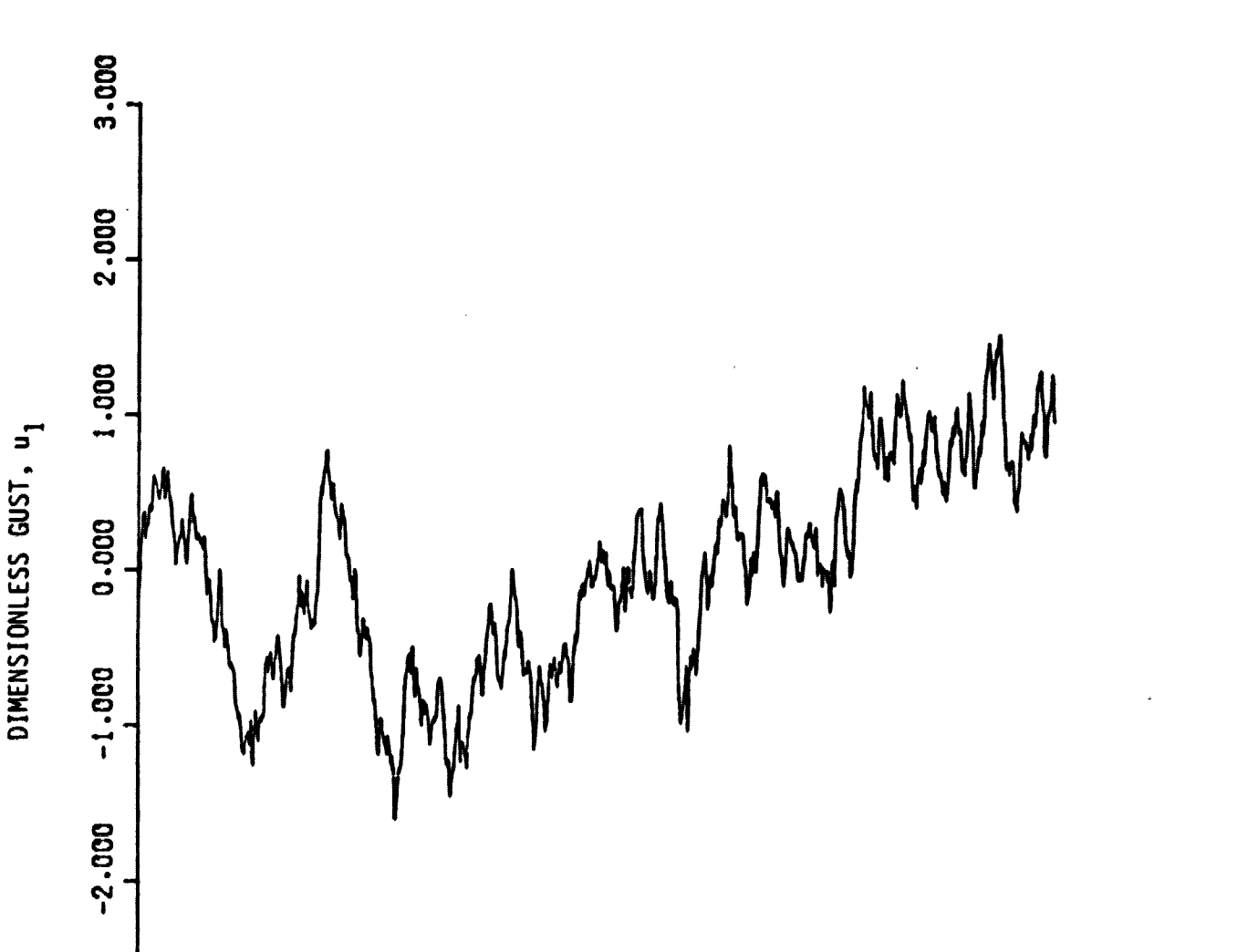

Figure 3-1. Sample Time Series for Turbulent Gust, u_1

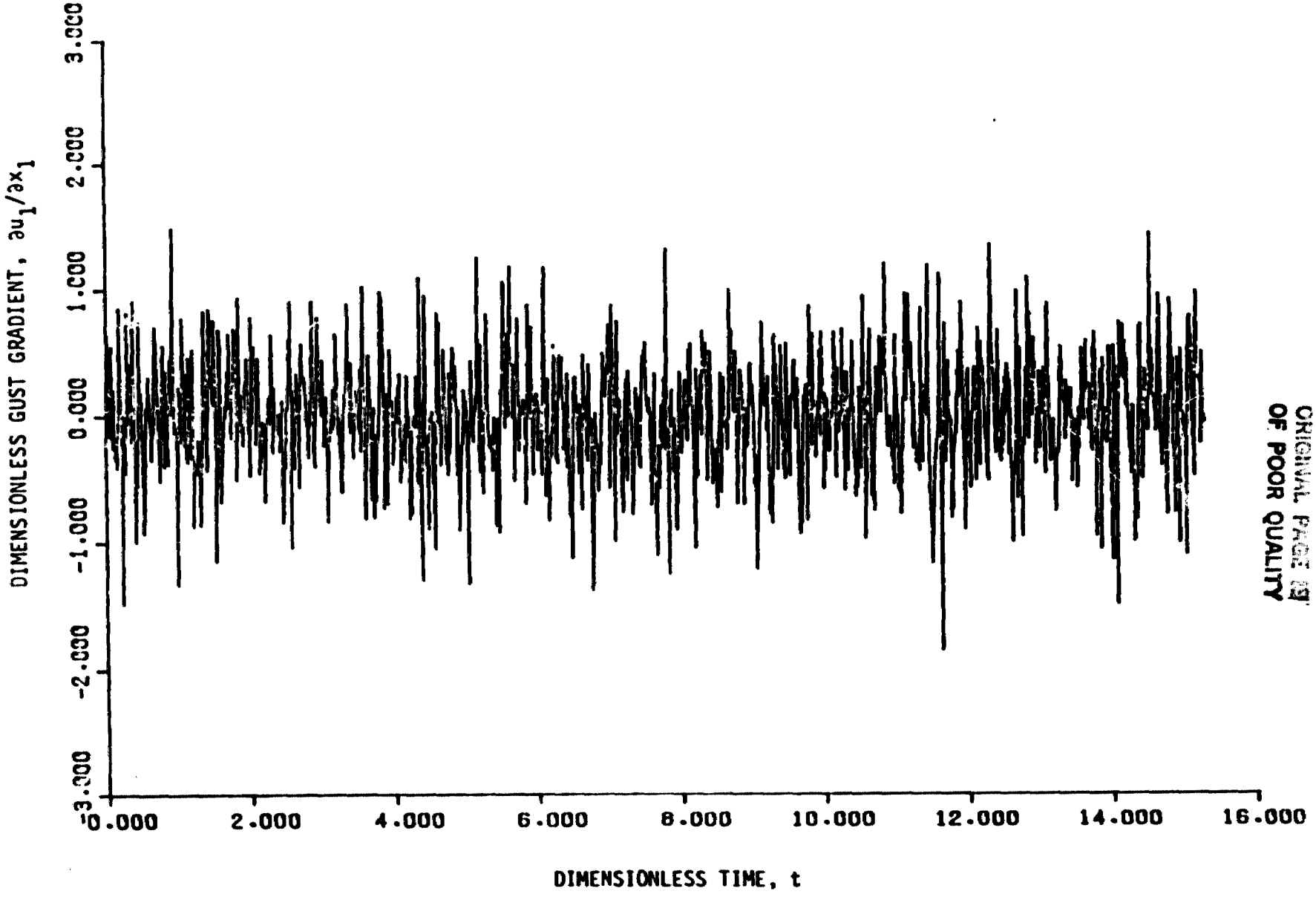

Figure 3-2. Sample Time Series for Turbulent Gust Gradient, $\partial u_1/\partial x_1$

TABLE 3-1. MAGNETIC TAPES FOR SIMULATED TURBULENCE TIME SERIES

Tape No.	Spectrum	Dimensionless Time Step	Number of Time Steps
1	Φ_{11}	.01047	30,000
2	Φ_{22}	.01102	30,000
3	Φ_{33}	.01102	30,000
4	$\Phi_{11/11}$	.01532	30,000
5	$\Phi_{11/22}$	.01208	30,000
6	$\Phi_{11/33}$	.01396	30,000
7	$\Phi_{22/11}$	.01628	30,000
8	$\Phi_{22/22}$	.01396	30,000
9	$\Phi_{22/33}$	.01461	30,000
10	$\Phi_{33/11}$	.01611	30,000
11	$\Phi_{33/22}$	.01282	30,000
12	$\Phi_{33/33}$	.01496	30,000

TABLE 3-2. MAGNETIC TAPE CHARACTERISTICS

Number of Tracks:	9
Header Type:	non-label
Character Type:	ASCII
Recording Density:	800 bits per inch

4. CONCLUSIONS AND RECOMMENDATIONS

A turbulence simulation model for gusts and gust gradients based on von Karman spectra with finite upper limits has been developed. In the development of the model the initial approach involving the use of a recursive model, based on digital filter simulation theory and meromorphic function series approximation, was not successful due to the unstable behavior of the resulting difference equations. The second approach, involving the use of a non-recursive model based on the impulse response function of the square root of each spectra, proved successful and forms the basis for the model which is incorporated into a digital computer program entitled TBSIM.

By means of TBSIM a time series has been generated for each of the three gust spectra and nine gust gradient spectra. Each time series has been recorded on a separate magnetic tape. These tapes are set up in such a manner as to be interfaced with other simulation programs.

The time series as currently generated appear representative of the turbulent gusts and gust gradients under consideration. The need exists, however, to subject each series to spectral analysis by means of Fourier transform to establish the degree to which atmospheric turbulence is actually simulated. In addition to such analysis a need also exists to determine whether or not the conversion of the time series from dimensionless to dimensional form poses any problem for a potential user.

5. REFERENCES CITED

1. Tatom, Frank B., and Smith, S. Ray, "Shuttle Orbiter Turbulence Simulation Model Development", *Summary Report, EAI-TR-79-001,* Engineering Analysis, Inc., Huntsville, Alabama, March 27, 1979.

2. Neuman, Frank, and Foster, John D., "Investigation of a Digital Automatic Aircraft Landing System in Turbulence", *NASA TN D-66066,* National Aeronautics and Space Administration, Washington, D.C., October 1970.

3. Tatom, Frank B., Lillard, Virginic C., and Bhalla, Lalit M., "Simultaneous Solution of Non-Linear Algebraic Equations", *Interim Technical Report E20-177,* Northrop Space Laboratories, Huntsville, Alabama, March 9, 1966.

4. Fichtl, George H., "A Technique for Simulating Turbulence for Aerospace Vehicle Flight Simulation Studies", *NASA TM 78141,* George C. Marshall Space Flight Center, Marshall Space Flight Center, Alabama, November 1977.

5. Fichtl, George H., Personal Communication, 2 June 1979.

6. Etkin, B., *Dynamics of Atmospheric Flight,* John Wiley & Sons, Inc., New York, 1972.

7. Tatom, Frank B., and King, Richard L., "Turbulence Simulation Mechanization for Space Shuttle Orbiter Dynamics and Control Studies", *SAI-780766-HU,* December 1977.

8. Space Shuttle Program Office, "Program Status Report", Lyndon B. Johnson Space Center, Houston, Texas, March 31, 1979.

9. Perlmutter, Morris, "Stochastic Simulation of Ocean Waves for SRB Simulation", *NASA TR-230-1446*, George C. Marshall Space Flight Center, Marshall Space Flight Center, Alabama, May 1975.

10. Fichtl, George H., Perlmutter, Morris, and Frost, Walter, "Monte Carlo Turbulence Simulation", *Handbook of Turbulence,* Vol. 1, Chapter 14, Plenum Publishing Corporation, 1977.

11. Davis, Philip J., and Rabinowitz, Philip, *Methods of Numerical Integration,* Academic Press, 1975.

APPENDIX A

VON KARMAN GUST AND GUST GRADIENT SPECTRA WITH FINITE UPPER LIMITS

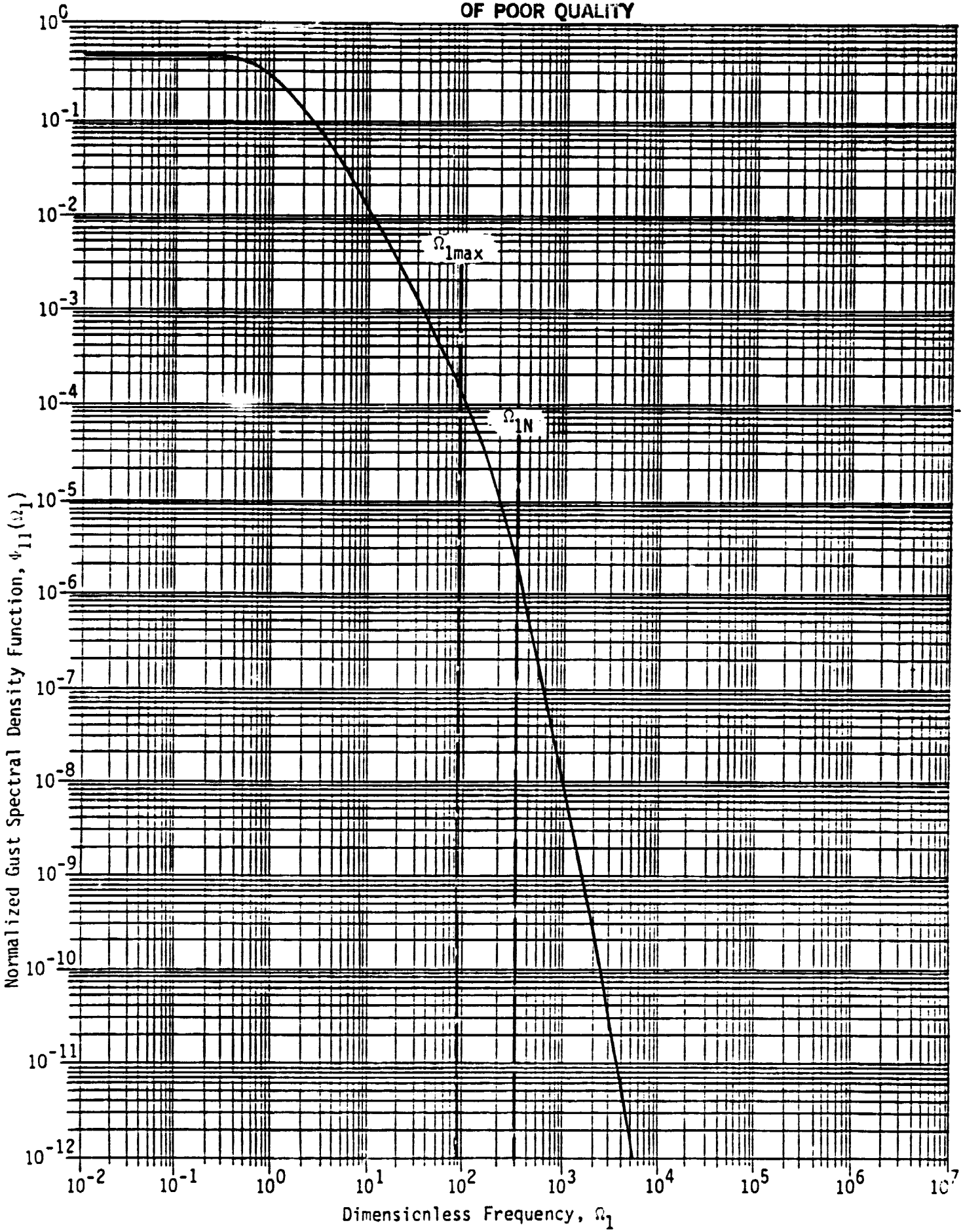

Figure A-1. Normalized Gust Spectra, $\Psi_{11}(\Omega_1)$

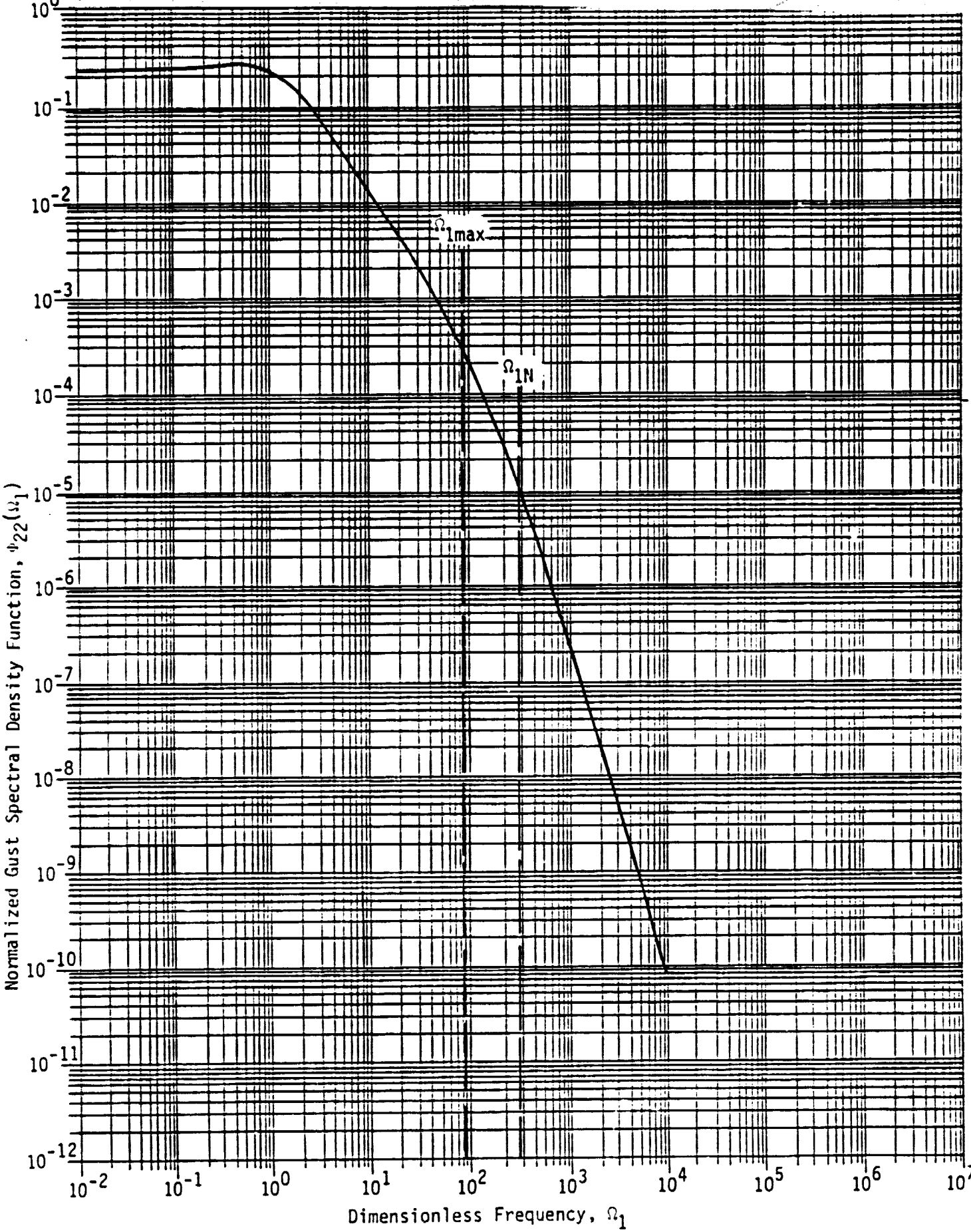

Figure A-2. Normalized Gust Spectra, $\Phi_{22}(\Omega_1)$

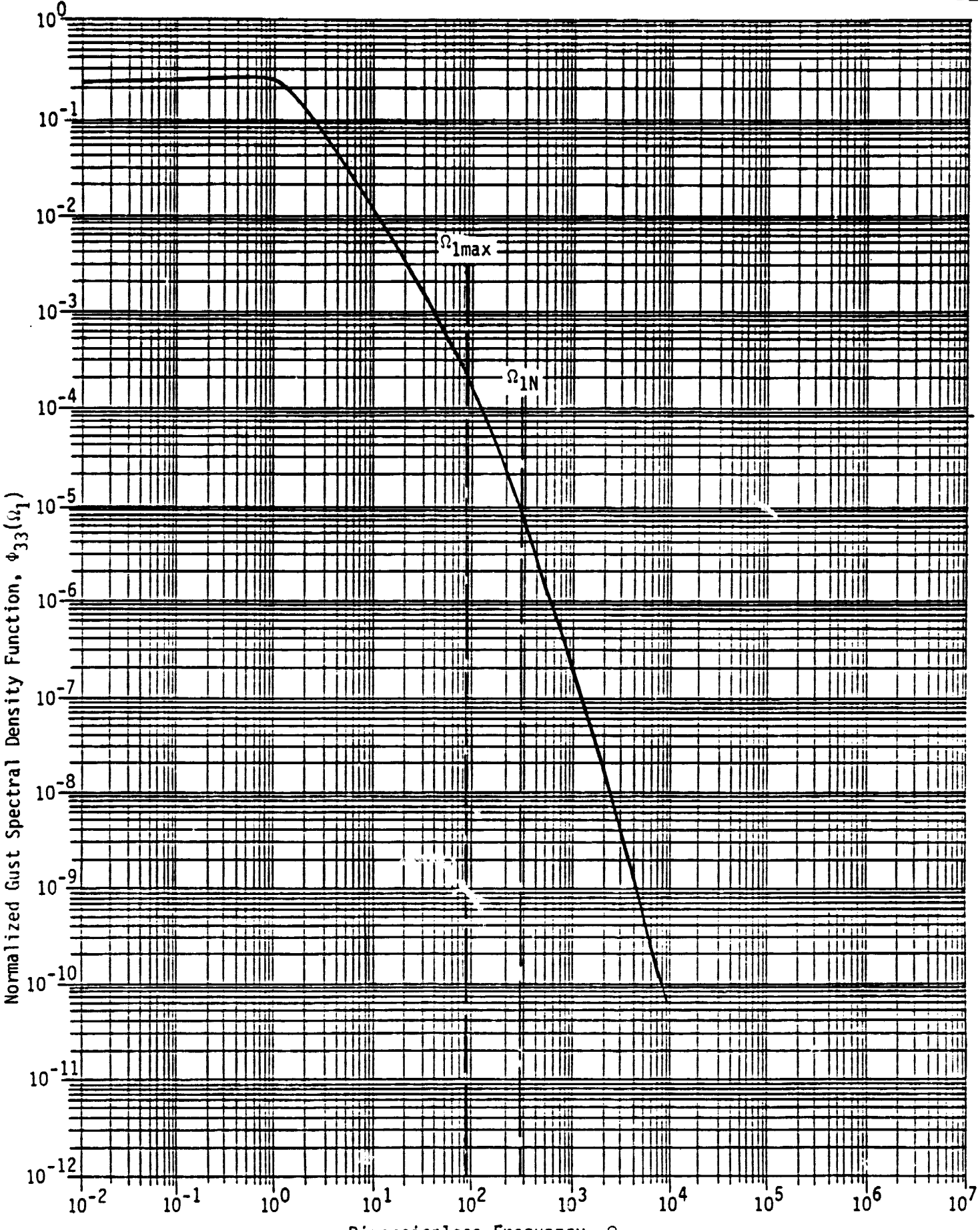

Figure A-3. Normalized Gust Spectra, $\Phi_{33}(\Omega_1)$

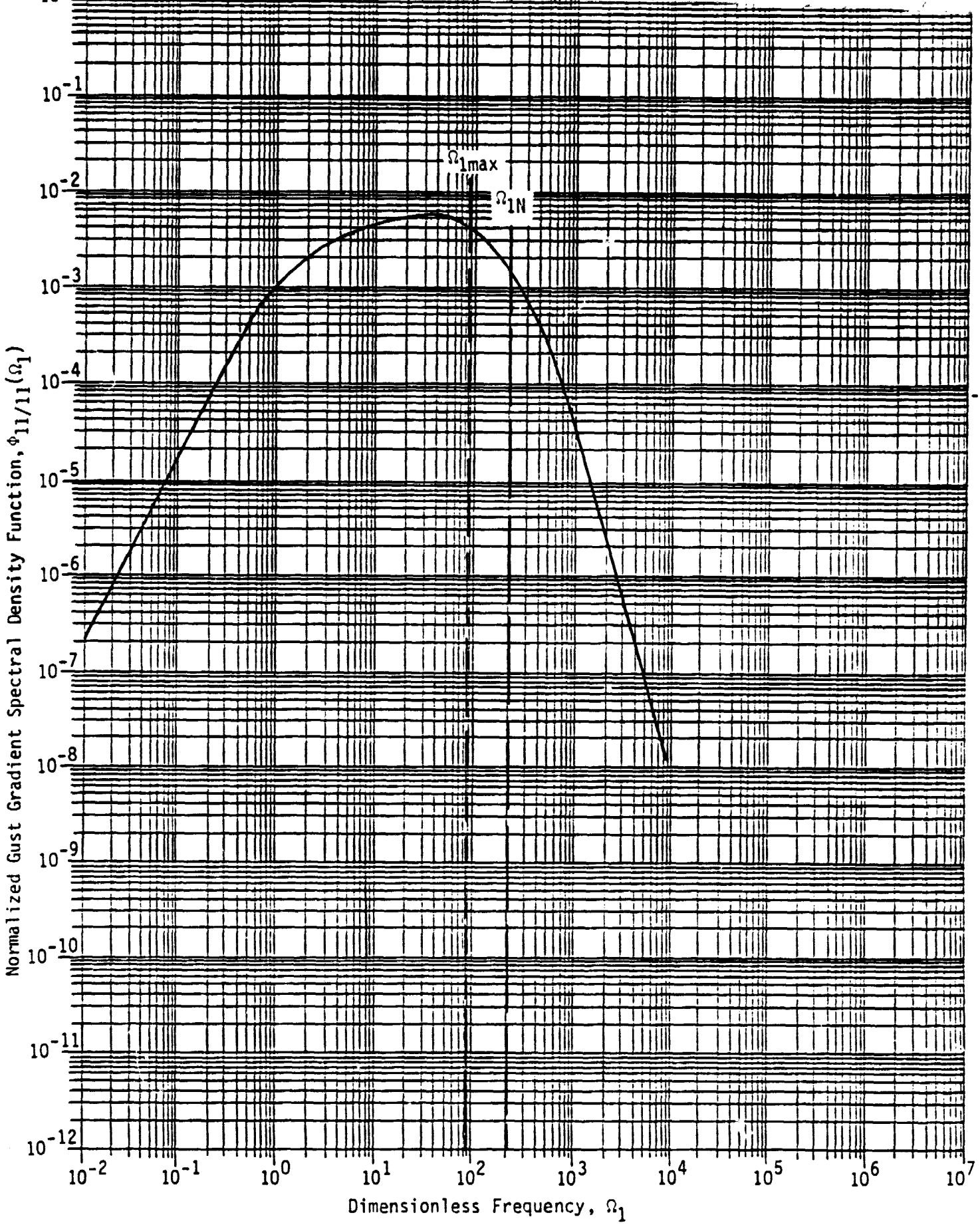

Figure A-4. Normalized Gust Gradient Spectra, $\Phi_{11/11}(\Omega_1)$

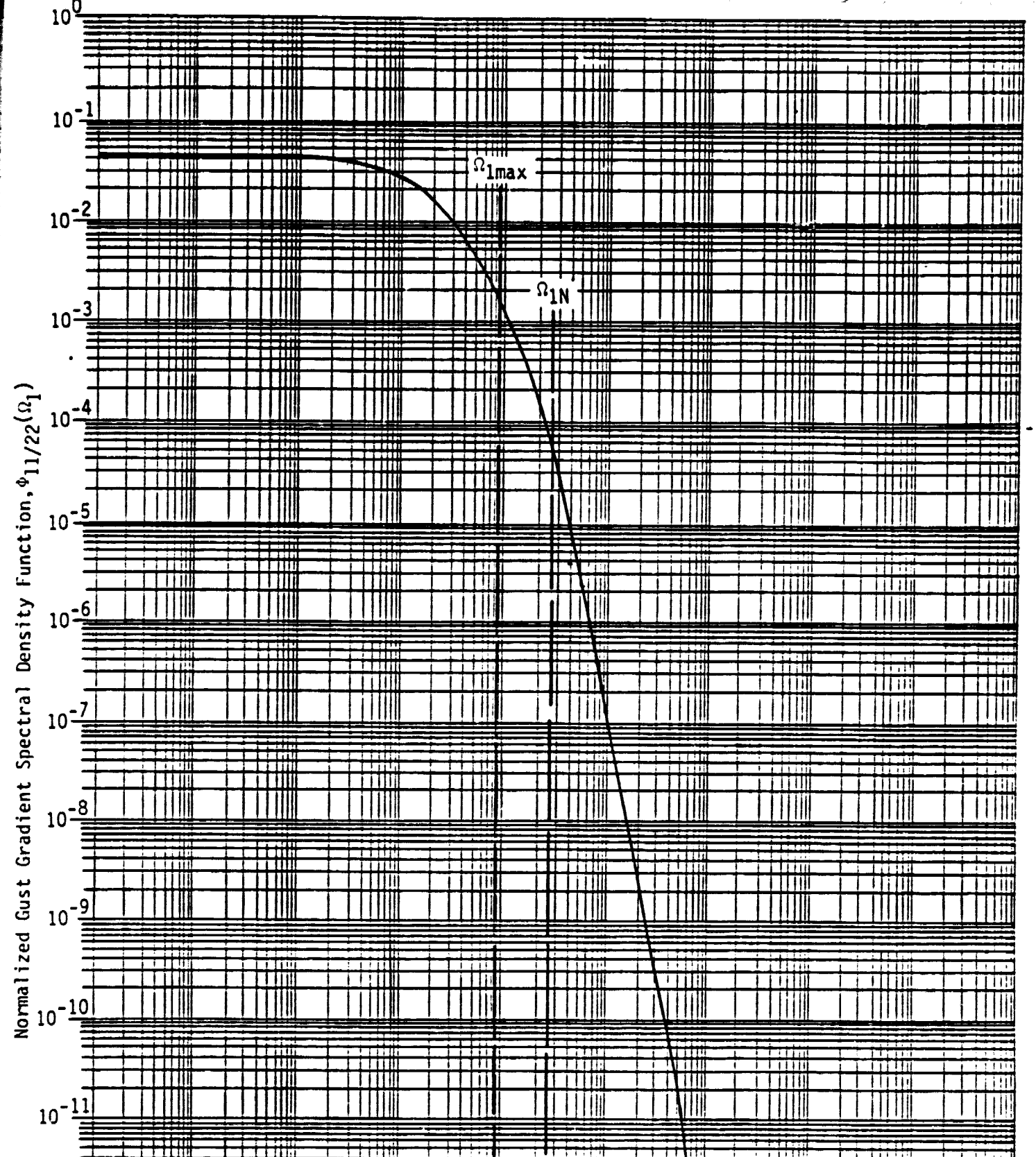

Figure A-5. Normalized Gust Gradient Spectra, $\Phi_{11/22}(\Omega_1)$

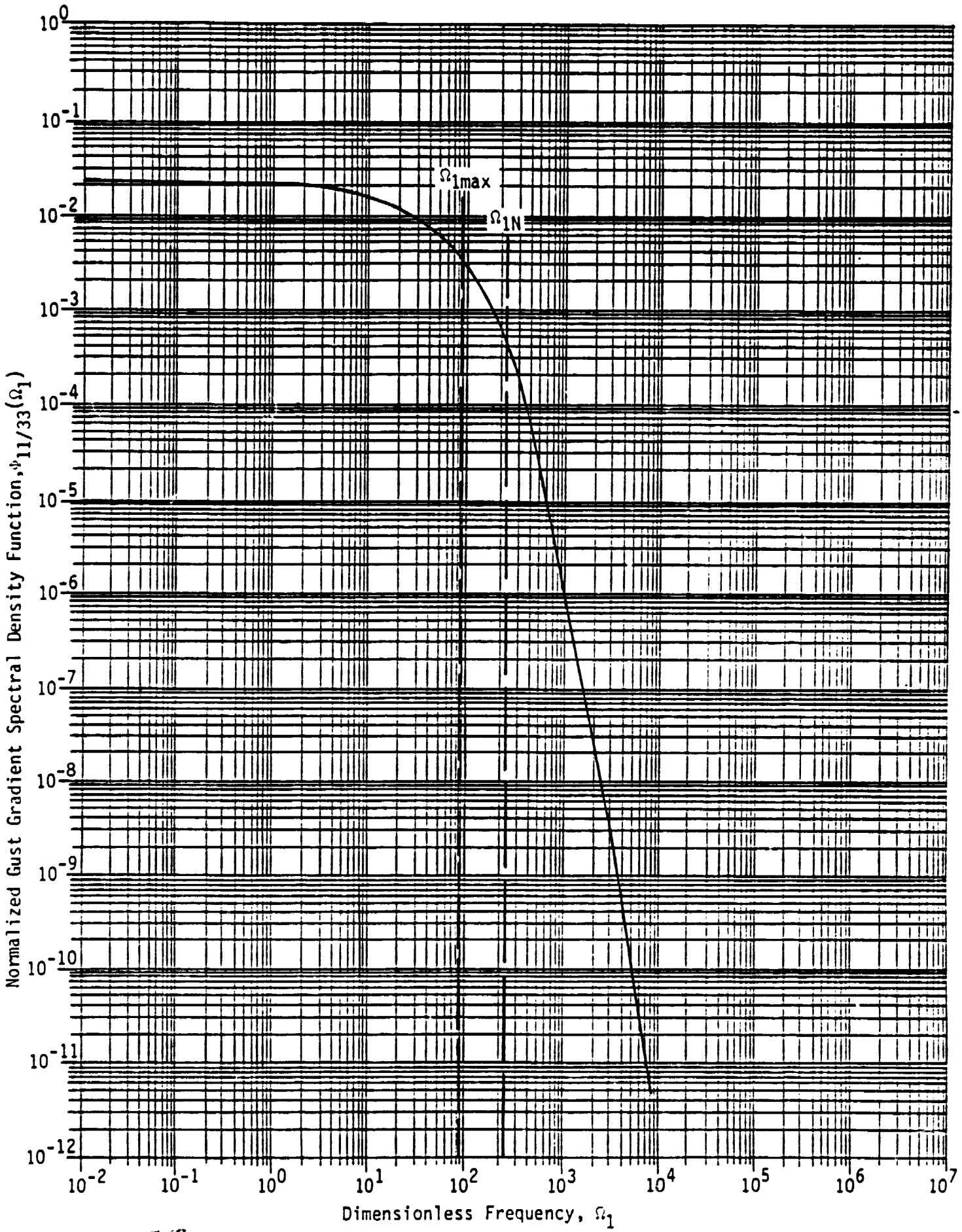

Figure A-6. Normalized Gust Gradient Spectra, $\Phi_{11/33}(\Omega_1)$

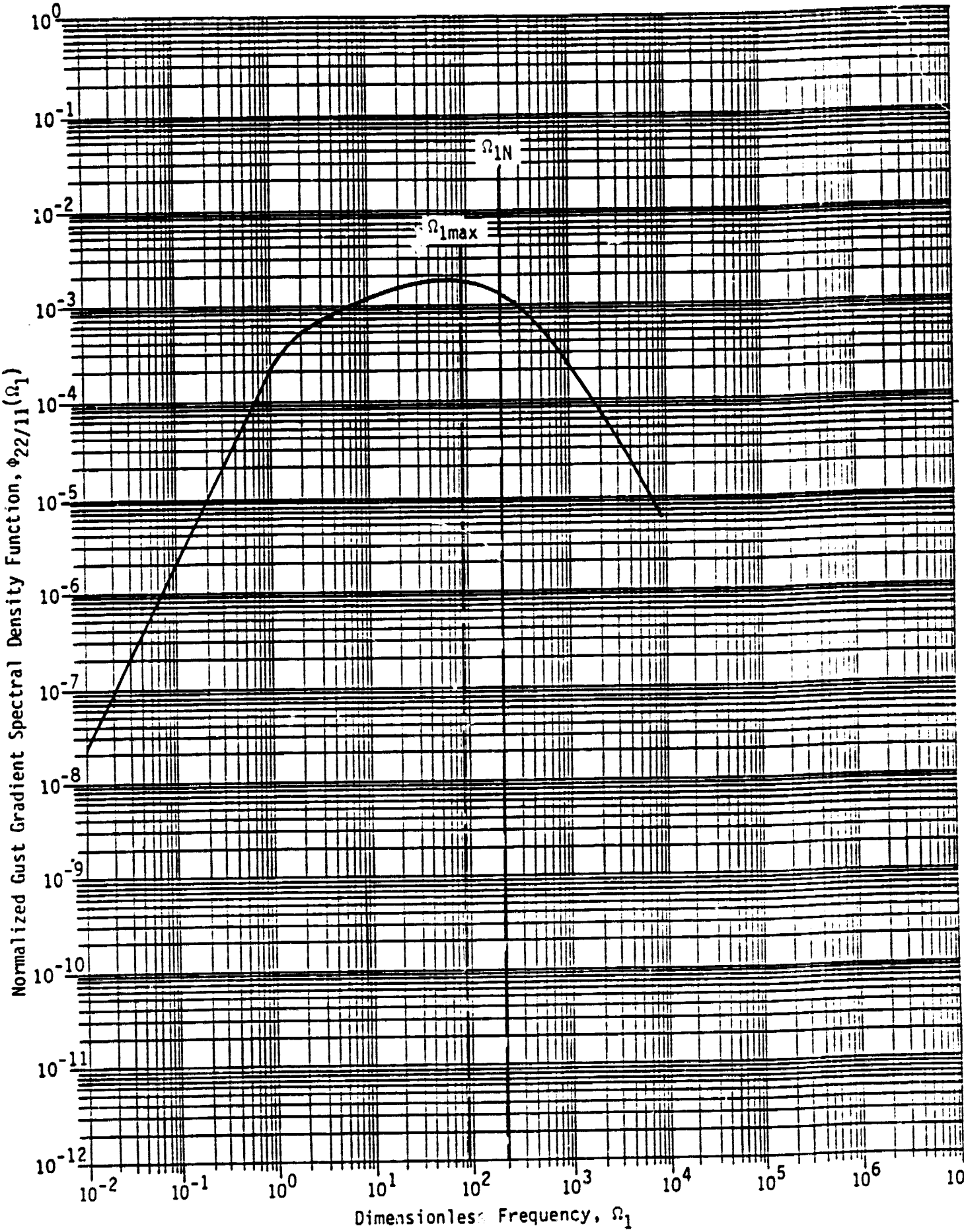

Figure A-7. Normalized Gust Gradient Spectra, $\Phi_{22/11}(\Omega_1)$

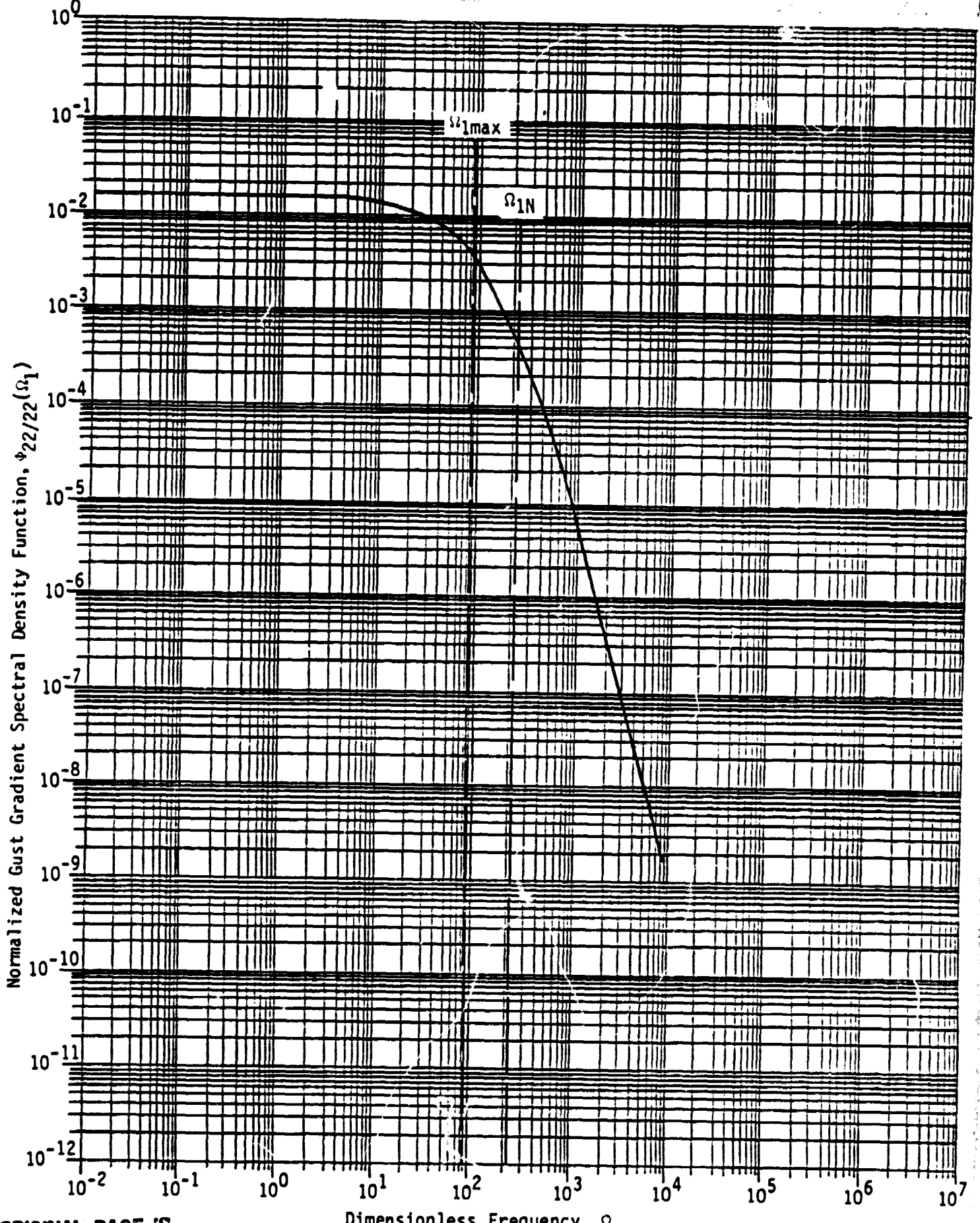

Figure A-8. Normalized Gust Gradient Spectra, $\Phi_{22/22}(\Omega_1)$

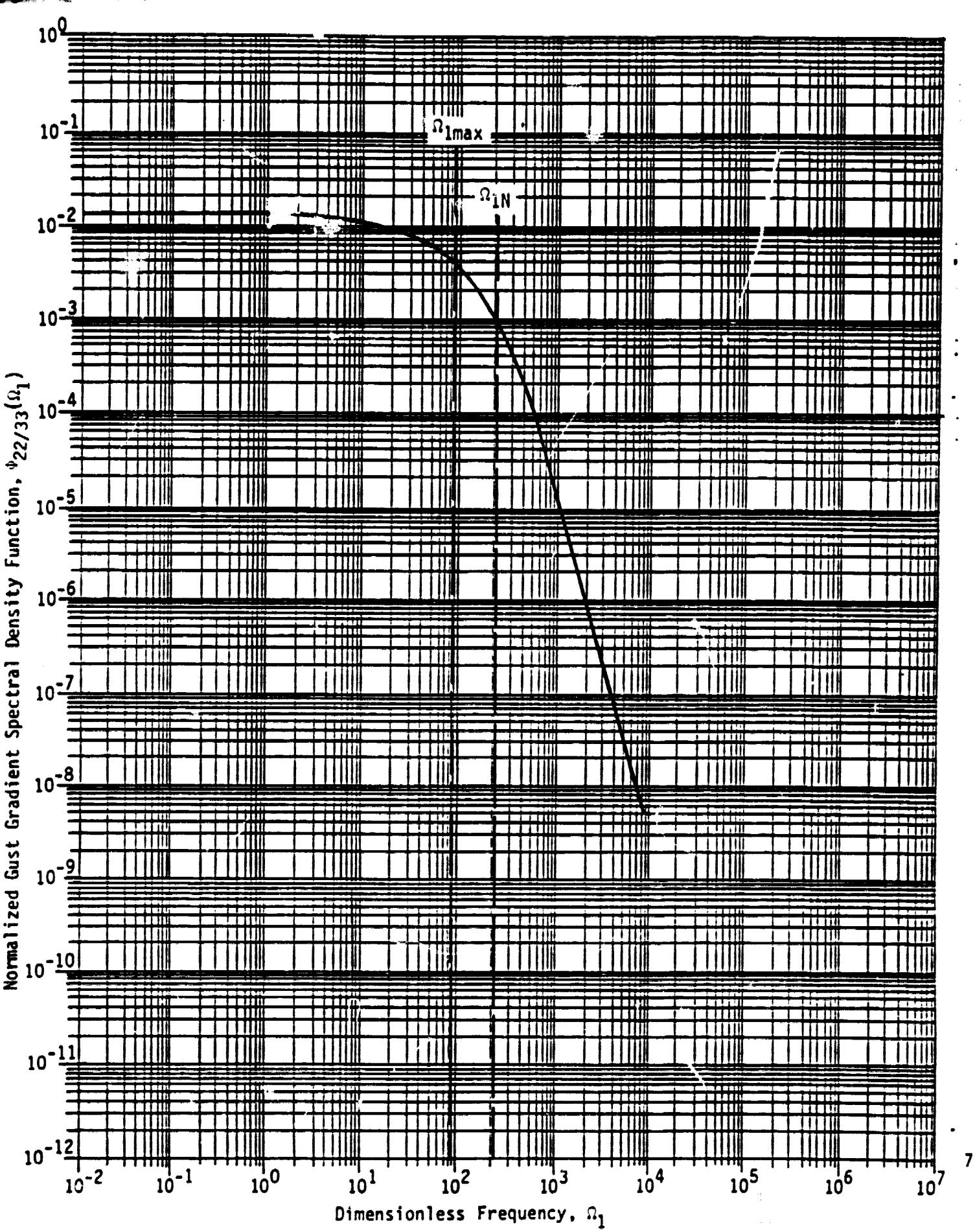

Figure A-9. Normalized Gust Gradient Spectra, $\Phi_{22/33}(\Omega_1)$

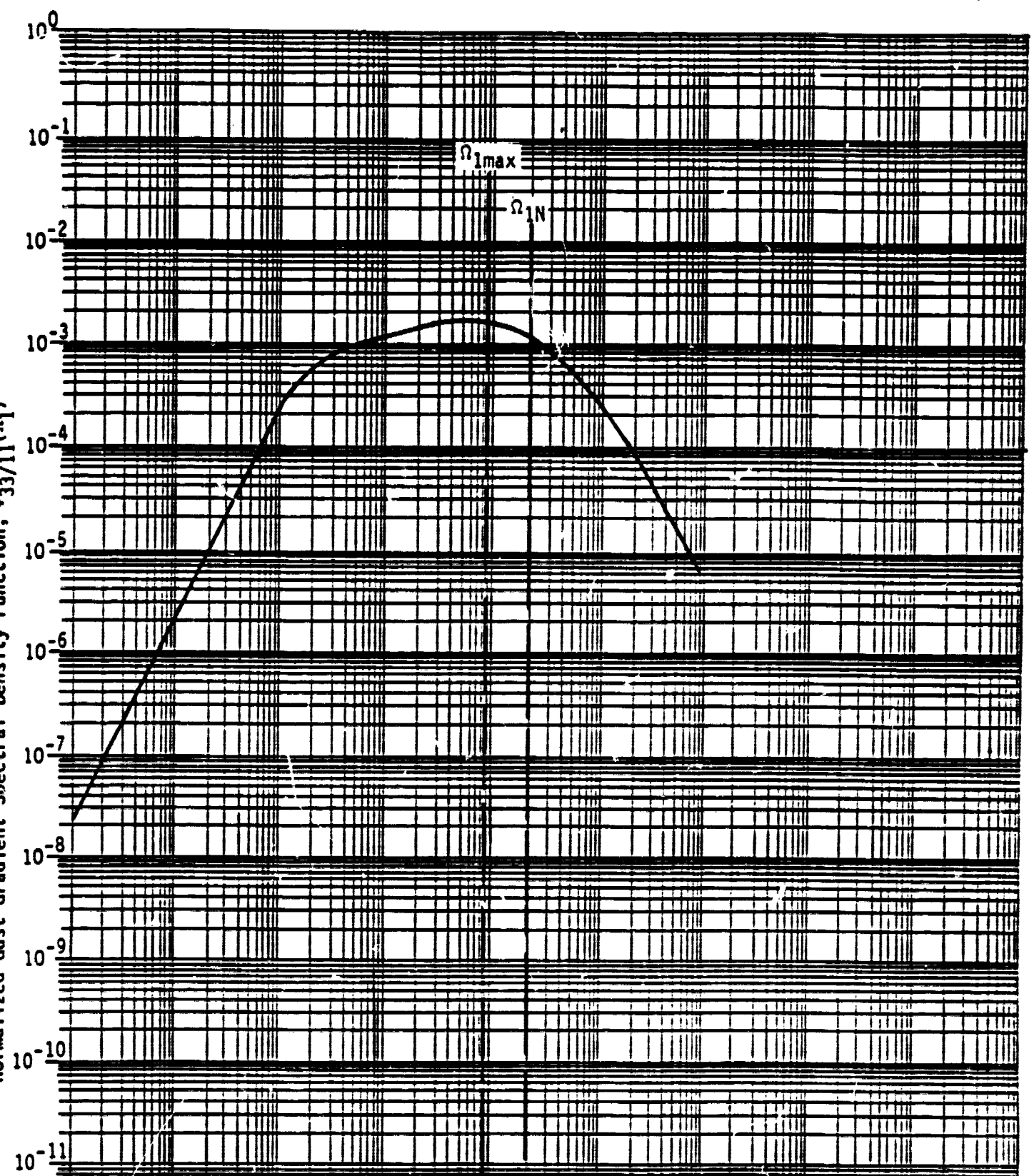

Figure A-10. Normalized Gust Gradient Spectra, $\Phi_{33/11}(\Omega_1)$

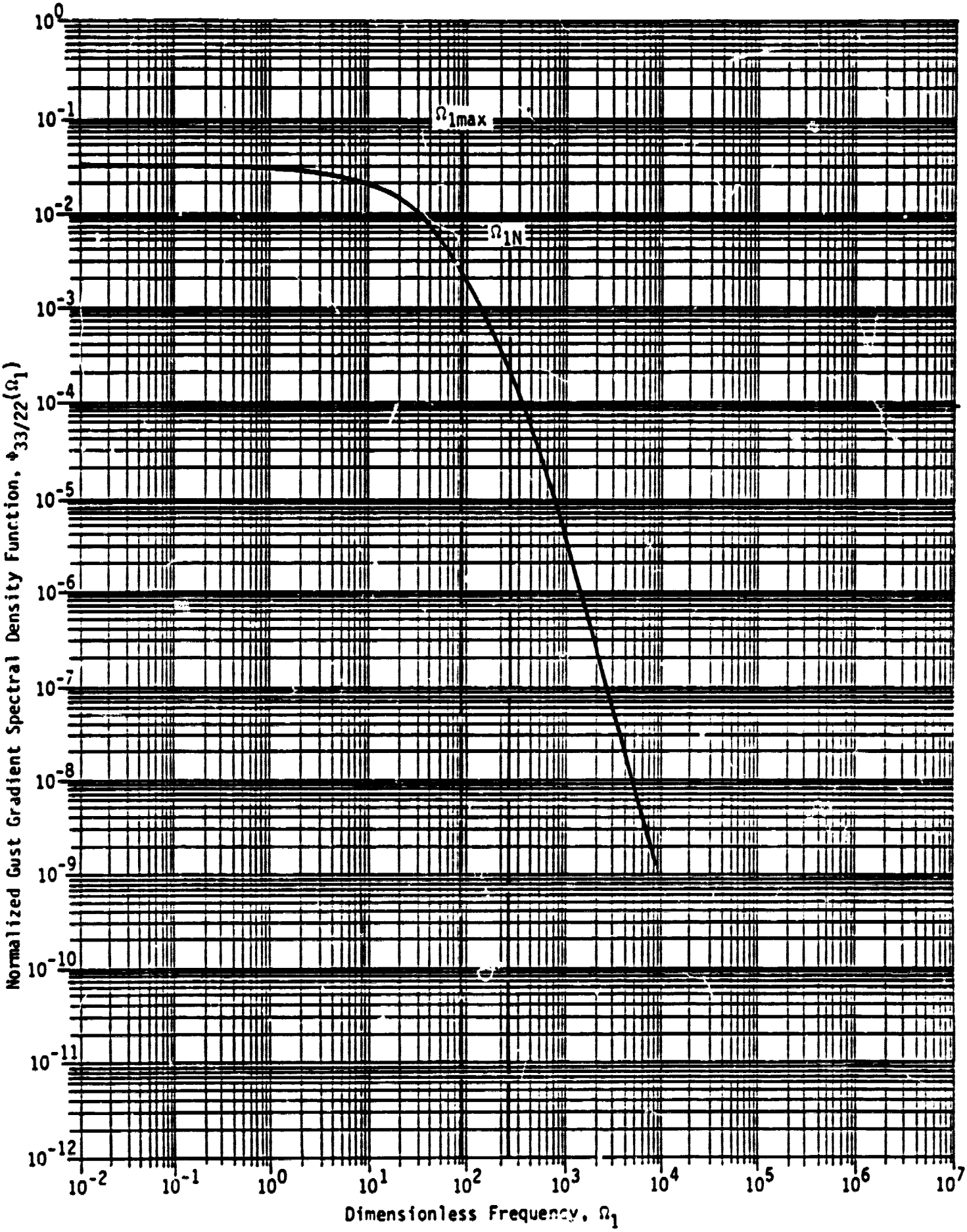

Figure A-11. Normalized Gust Gradient Spectra, $\Phi_{33/22}(\Omega_1)$

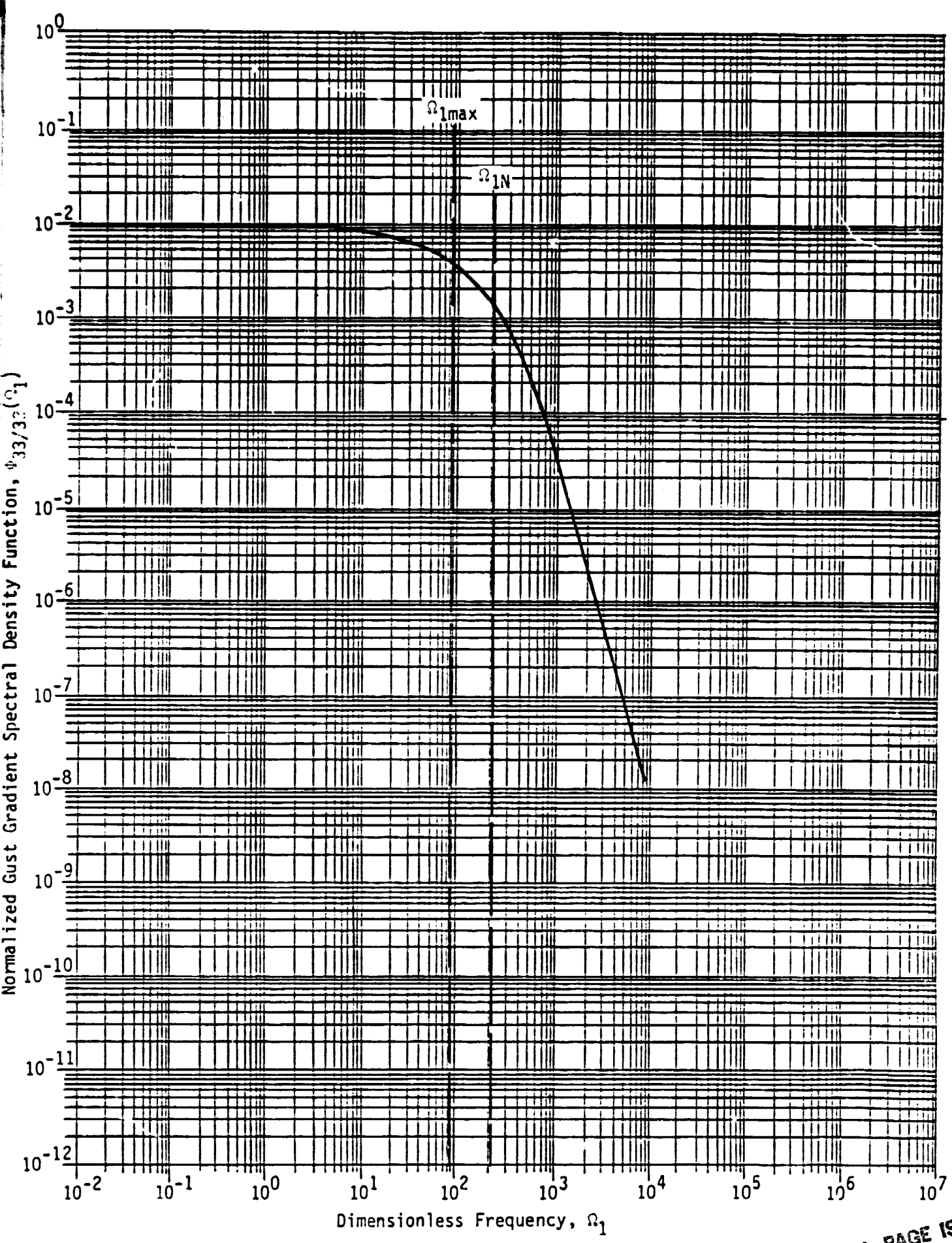

Figure A-12. Normalized Gust Gradient Spectra, $\Phi_{33/33}(\Omega_1)$

APPENDIX B

COMPARISON BETWEEN MODIFIED AND ORIGINAL SPECTRA

TABLE B-1. Φ_{11} SPECTRA FOR Ω_{1N} = 300.0

Ω_1	Φ'	Φ	Φ'/Φ
.1000E-05	.4746	.4746	1.000
1.0000E-02	.4745	.4745	1.000
.2000E-01	.4744	.4744	1.000
.3000E-01	.4742	.4742	1.000
.4000E-01	.4739	.4739	1.000
.5000E-01	.4736	.4736	1.000
.6000E-01	.4732	.4732	1.000
.7000E-01	.4726	.4726	1.000
.8000E-01	.4720	.4720	1.000
.9000E-01	.4714	.4714	1.000
1.0000E-01	.4706	.4706	1.000
.1900	.4606	.4606	1.000
.2800	.4453	.4453	1.000
.3700	.4260	.4260	1.000
.4600	.4038	.4038	1.000
.5500	.3801	.3801	1.000
.6400	.3558	.3558	1.000
.7300	.3317	.3317	1.000
.8200	.3086	.3086	1.000
.9100	.2866	.2866	1.0000
1.000	.2661	.2661	1.0000
1.900	.1337	.1337	.9999
2.800	.7789E-01	.7790E-01	.9998
3.700	.5098E-01	.5100E-01	.9997
4.600	.3609E-01	.3611E-01	.9995
5.500	.2698E-01	.2700E-01	.9993
6.400	.2097E-01	.2100E-01	.9990
7.300	.1681E-01	.1683E-01	.9987
8.200	.1379E-01	.1382E-01	.9983
9.100	.1154E-01	.1157E-01	.9980
10.000	.9817E-02	.9841E-02	.9975
19.00	.3201E-02	.3227E-02	.9919
28.00	.1555E-02	.1579E-02	.9852
37.00	.8938E-03	.9112E-03	.9810
46.00	.5675E-03	.5766E-03	.9842
55.00	.3879E-03	.3871E-03	1.002
64.00	.2829E-03	.2712E-03	1.043
73.00	.2202E-03	.1962E-03	1.123
82.00	.1955E-03	.1457E-03	1.342
86.30	.1948E-03	.1289E-03	1.511

$$\frac{\int_0^{\Omega_{1max}} \Phi'(\Omega_1)\,d\Omega_1}{\int_0^{\Omega_{1max}} \Phi(\Omega_1)\,d\Omega_1} = \frac{.94730}{.94773} = .99954$$

TABLE B-2. Φ_{22} SPECTRA FOR Ω_{1N} = 285.0

Ω_1	Φ'	Φ	Φ'/Φ
.1000E-05	.2374	.2374	1.000
1.0000E-02	.2374	.2374	1.000
.2000E-01	.2375	.2375	1.000
.3000E-01	.2376	.2376	1.000
.4000E-01	.2377	.2377	1.000
.5000E-01	.2379	.2379	1.000
.6000E-01	.2382	.2381	1.000
.7000E-01	.2384	.2384	1.000
.8000E-01	.2387	.2387	1.000
.9000E-01	.2390	.2390	1.000
1.0000E-01	.2394	.2394	1.000
.1900	.2441	.2441	1.000
.2800	.2503	.2503	1.000
.3700	.2567	.2567	1.000
.4600	.2620	.2620	1.000
.5500	.2651	.2651	1.000
.6400	.2657	.2657	1.000
.7300	.2637	.2637	1.000
.8200	.2594	.2594	1.000
.9100	.2530	.2530	1.000
1.000	.2452	.2452	1.000
1.900	.1536	.1536	1.0000
2.800	.9619E-01	.9620E-01	.9999
3.700	.6504E-01	.6505E-01	.9998
4.600	.4692E-01	.4693E-01	.9996
5.500	.3554E-01	.3556E-01	.9994
6.400	.2794E-01	.2796E-01	.9992
7.300	.2259E-01	.2261E-01	.9990
8.200	.1868E-01	.1870E-01	.9987
9.100	.1573E-01	.1575E-01	.9984
10.000	.1344E-01	.1347E-01	.9980
19.00	.4548E-02	.4576E-02	.9938
28.00	.2338E-02	.2362E-02	.9900
37.00	.1438E-02	.1452E-02	.9901
46.00	.9813E-03	.9825E-03	.9989
55.00	.7214E-03	.7057E-03	1.022
64.00	.5636E-03	.5281E-03	1.067
73.00	.4660E-03	.4071E-03	1.145
82.00	.4273E-03	.3210E-03	1.331
86.30	.4260E-03	.2908E-03	1.465

$$\frac{\int_0^{\Omega_{1max}} \Phi'(\Omega_1)\,d\Omega_1}{\int_0^{\Omega_{1max}} \Phi(\Omega_1)\,d\Omega_1} = \frac{.94794}{.94739} = 1.0006$$

TABLE B-3. Φ_{33} SPECTRA FOR Ω_{1N} = 285.0

Ω_1	Φ'	Φ	Φ'/Φ
.1000E-05	.2372	.2372	1.000
1.0000E-02	.2372	.2372	1.000
.2000E-01	.2373	.2373	1.000
.3000E-01	.2374	.2373	1.000
.4000E-01	.2375	.2375	1.000
.5000E-01	.2377	.2377	1.000
.6000E-01	.2379	.2379	1.000
.7000E-01	.2382	.2382	1.000
.8000E-01	.2385	.2384	1.000
.9000E-01	.2388	.2388	1.000
1.0000E-01	.2392	.2391	1.000
.1900	.2438	.2438	1.000
.2800	.2501	.2501	1.000
.3700	.2565	.2565	1.000
.4600	.2617	.2617	1.000
.5500	.2649	.2649	1.000
.6400	.2655	.2655	1.000
.7300	.2635	.2635	1.000
.8200	.2591	.2591	1.000
.9100	.2528	.2528	1.000
1.000	.2450	.2450	1.000
1.900	.1534	.1534	1.0000
2.800	.9599E-01	.9600E-01	.9999
3.700	.6486E-01	.6488E-01	.9997
4.600	.4676E-01	.4679E-01	.9995
5.500	.3541E-01	.3543E-01	.9993
6.400	.2782E-01	.2784E-01	.9991
7.300	.2248E-01	.2251E-01	.9988
8.200	.1857E-01	.1860E-01	.9985
9.100	.1563E-01	.1565E-01	.9981
10.000	.1334E-01	.1337E-01	.9977
19.00	.4431E-02	.4464E-02	.9926
28.00	.2228E-02	.2257E-02	.9872
37.00	.1337E-02	.1357E-02	.9853
46.00	.8904E-03	.8980E-03	.9916
55.00	.6396E-03	.6316E-03	1.013
64.00	.4897E-03	.4637E-03	1.056
73.00	.3985E-03	.3516E-03	1.133
82.00	.3623E-03	.2734E-03	1.325
86.30	.3611E-03	.2465E-03	1.465

$$\frac{\int_0^{\Omega_{1max}} \Phi'(\Omega_1)\,d\Omega_1}{\int_0^{\Omega_{1max}} \Phi(\Omega_1)\,d\Omega_1} = \frac{.93981}{.93985} = .99996$$

TABLE B-4. $\Phi_{11/11}$ SPECTRA FOR Ω_{1N} = 205.0

Ω_1	Φ'	Φ	Φ'/Φ
.1000E-05	.7190E-04	.2035E-10	.3533E+07
1.0000E-02	.7216E-04	.2035E-06	354.6
.2000E-01	.7282E-04	.8137E-06	89.50
.3000E-01	.7390E-04	.1830E-05	40.38
.4000E-01	.7537E-04	.3252E-05	23.18
.5000E-01	.7725E-04	.5077E-05	15.22
.6000E-01	.7954E-04	.7304E-05	10.89
.7000E-01	.8222E-04	.9931E-05	8.279
.8000E-01	.8530E-04	.1295E-04	6.584
.9000E-01	.8877E-04	.1637E-04	5.422
1.0000E-01	.9264E-04	.2018E-04	4.590
.1900	.1443E-03	.7130E-04	2.023
.2800	.2232E-03	.1497E-03	1.491
.3700	.3240E-03	.2501E-03	1.296
.4600	.4409E-03	.3664E-03	1.203
.5500	.5680E-03	.4930E-03	1.152
.6400	.7004E-03	.6249E-03	1.121
.7300	.8341E-03	.7581E-03	1.100
.8200	.9662E-03	.8897E-03	1.086
.9100	.1095E-02	.1018E-02	1.076
1.000	.1218E-02	.1141E-02	1.068
1.900	.2151E-02	.2069E-02	1.040
2.800	.2706E-02	.2619E-02	1.033
3.700	.3085E-02	.2994E-02	1.030
4.600	.3372E-02	.3277E-02	1.029
5.500	.3600E-02	.3502E-02	1.028
6.400	.3789E-02	.3688E-02	1.028
7.300	.3950E-02	.3846E-02	1.027
8.200	.4090E-02	.3984E-02	1.027
9.100	.4215E-02	.4107E-02	1.026
10.000	.4330E-02	.4220E-02	1.026
19.00	.5091E-02	.4995E-02	1.019
28.00	.5350E-02	.5307E-02	1.008
37.00	.5323E-02	.5349E-02	.9951
46.00	.5145E-02	.5232E-02	.9834
55.00	.4906E-02	.5022E-02	.9770
64.00	.4669E-02	.4763E-02	.9803
73.00	.4474E-02	.4483E-02	.9979
82.00	.4382E-02	.4201E-02	1.043
86.30	.43?2E-02	.4070E-02	1.074

$$\frac{\int_0^{\Omega_{1max}} \Phi'(\Omega_1)d\Omega_1}{\int_0^{\Omega_{1max}} \Phi(\Omega_1)d\Omega_1} = \frac{.38562}{.38530} = 1.0008$$

TABLE B-5. $\Phi_{11/22}$ SPECTRA FOR Ω_{1N} = 260.0

Ω_1	Φ'	Φ	Φ'/Φ
.1000E-05	.4276E-01	.4269E-01	1.002
1.0000E-02	.4276E-01	.4269E-01	1.002
.2000E-01	.4276E-01	.4269E-01	1.002
.3000E-01	.4276E-01	.4269E-01	1.002
.4000E-01	.4275E-01	.4269E-01	1.002
.5000E-01	.4275E-01	.4269E-01	1.002
.6000E-01	.4275E-01	.4268E-01	1.002
.7000E-01	.4275E-01	.4268E-01	1.002
.8000E-01	.4274E-01	.4267E-01	1.002
.9000E-01	.4274E-01	.4267E-01	1.002
1.0000E-01	.4273E-01	.4267E-01	1.002
.1900	.4266E-01	.4260E-01	1.002
.2800	.4255E-01	.4249E-01	1.002
.3700	.4241E-01	.4234E-01	1.002
.4600	.4223E-01	.4216E-01	1.002
.5500	.4203E-01	.4196E-01	1.002
.6400	.4180E-01	.4173E-01	1.002
.7300	.4156E-01	.4149E-01	1.002
.8200	.4130E-01	.4124E-01	1.002
.9100	.4104E-01	.4097E-01	1.002
1.000	.4077E-01	.4070E-01	1.002
1.900	.3801E-01	.3794E-01	1.002
2.800	.3557E-01	.3551E-01	1.002
3.700	.3348E-01	.3342E-01	1.002
4.600	.3166E-01	.3161E-01	1.002
5.500	.3005E-01	.3001E-01	1.001
6.400	.2861E-01	.2857E-01	1.001
7.300	.2730E-01	.2727E-01	1.001
8.200	.2610E-01	.2608E-01	1.001
9.100	.2499E-01	.2498E-01	1.000
10.000	.2396E-01	.2396E-01	.9997
19.00	.1631E-01	.1643E-01	.9923
28.00	.1146E-01	.1167E-01	.9815
37.00	.8187E-02	.8435E-02	.9706
46.00	.5951E-02	.6173E-02	.9641
55.00	.4427E-02	.4570E-02	.9687
64.00	.3401E-02	.3424E-02	.9932
73.00	.2731E-02	.2597E-02	1.052
82.00	.2455E-02	.1994E-02	1.231
86.30	.2445E-02	.1781E-02	1.372

$$\frac{\int_0^{\Omega_{1max}} \Phi'(\Omega_1)d\Omega_1}{\int_0^{\Omega_{1max}} \Phi(\Omega_1)d\Omega_1} = \frac{.90308}{.90866} = .99386$$

TABLE B-6. $\Phi_{11/33}$ SPECTRA FOR Ω_{1N} = 225.0

Ω_1	Φ'	Φ	Φ'/Φ
.1000E-05	.2243E-01	.2234E-01	1.004
1.0000E-02	.2243E-01	.2234E-01	1.004
.2000E-01	.2243E-01	.2233E-01	1.004
.3000E-01	.2243E-01	.2233E-01	1.004
.4000E-01	.2243E-01	.2233E-01	1.004
.5000E-01	.2242E-01	.2233E-01	1.004
.6000E-01	.2242E-01	.2233E-01	1.004
.7000E-01	.2242E-01	.2233E-01	1.004
.8000E-01	.2242E-01	.2233E-01	1.004
.9000E-01	.2242E-01	.2233E-01	1.004
1.0000E-01	.2242E-01	.2232E-01	1.004
.1900	.2239E-01	.2230E-01	1.004
.2800	.2235E-01	.2226E-01	1.004
.3700	.2229E-01	.2220E-01	1.004
.4600	.2222E-01	.2213E-01	1.004
.5500	.2214E-01	.2205E-01	1.004
.6400	.2206E-01	.2196E-01	1.004
.7300	.2196E-01	.2187E-01	1.004
.8200	.2186E-01	.2177E-01	1.004
.9100	.2176E-01	.2166E-01	1.004
1.000	.2165E-01	.2156E-01	1.004
1.900	.2058E-01	.2048E-01	1.005
2.800	.1963E-01	.1953E-01	1.005
3.700	.1881E-01	.1871E-01	1.005
4.600	.1810E-01	.1800E-01	1.005
5.500	.1746E-01	.1737E-01	1.005
6.400	.1690E-01	.1681E-01	1.005
7.300	.1638E-01	.1629E-01	1.005
8.200	.1590E-01	.1582E-01	1.005
9.100	.1546E-01	.1539E-01	1.005
10.000	.1504E-01	.1498E-01	1.004
19.00	.1184E-01	.1187E-01	.9976
28.00	.9611E-02	.9735E-02	.9873
37.00	.7940E-02	.8131E-02	.9766
46.00	.6660E-02	.6869E-02	.9696
55.00	.5684E-02	.5850E-02	.9715
64.00	.4956E-02	.5014E-02	.9883
73.00	.4441E-02	.4320E-02	1.028
82.00	.4222E-02	.3738E-02	1.129
86.30	.4207E-02	.3503E-02	1.201

$$\frac{\int_0^{\Omega_{1max}} \Phi'(\Omega_1)\,d\Omega_1}{\int_0^{\Omega_{1max}} \Phi(\Omega_1)\,d\Omega_1} = \frac{.72592}{.72890} = .99590$$

TABLE B-7. $\Phi_{22/11}$ SPECTRA FOR Ω_{1N} = 193.0

Ω_1	Φ'	Φ	Φ'/Φ
.1000E-05	.2024E-04	.2096E-11	.9656E+07
1.0000E-02	.2028E-04	.2096E-07	967.6
.2000E-01	.2037E-04	.8387E-07	242.9
.3000E-01	.2050E-04	.1888E-06	108.6
.4000E-01	.2066E-04	.3358E-06	61.54
.5000E-01	.2088E-04	.5251E-06	39.76
.6000E-01	.2113E-04	.7569E-06	27.92
.7000E-01	.2143E-04	.1031E-05	20.78
.8000E-01	.2177E-04	.1349E-05	16.14
.9000E-01	.2215E-04	.1709E-05	12.96
1.0000E-01	.2258E-04	.2113E-05	10.68
.1900	.2844E-04	.7779E-05	3.656
.2800	.3819E-04	.1733E-04	2.204
.3700	.5209E-04	.3103E-04	1.679
.4600	.7021E-04	.4894E-04	1.435
.5500	.9228E-04	.7080E-04	1.303
.6400	.1178E-03	.9609E-04	1.226
.7300	.1460E-03	.1241E-03	1.176
.8200	.1760E-03	.1540E-03	1.143
.9100	.2073E-03	.1850E-03	1.121
1.000	.2390E-03	.2165E-03	1.104
1.900	.5141E-03	.4896E-03	1.050
2.800	.6924E-03	.6659E-03	1.040
3.700	.8147E-03	.7862E-03	1.036
4.600	.9071E-03	.8768E-03	1.035
5.500	.9818E-03	.9497E-03	1.034
6.400	.1045E-02	.1011E-02	1.033
7.300	.1099E-02	.1064E-02	1.033
8.200	.1147E-02	.1110E-02	1.033
9.100	.1190E-02	.1152E-02	1.033
10.000	.1229E-02	.1189E-02	1.033
19.00	.1504E-02	.1458E-02	1.031
28.00	.1673E-02	.1635E-02	1.024
37.00	.1776E-02	.1755E-02	1.012
46.00	.1833E-02	.1835E-02	.9990
55.00	.1860E-02	.1885E-02	.9870
64.00	.1869E-02	.1910E-02	.9790
73.00	.1872E-02	.1915E-02	.9774
82.00	.1870E-02	.1906E-02	.9814
86.30	.1869E-02	.1896E-02	.9858

$$\frac{\int_0^{\Omega_{1max}} \Phi'(\Omega_1)\,d\Omega_1}{\int_0^{\Omega_{1max}} \Phi(\Omega_1)\,d\Omega_1} = \frac{.13403}{.13375} = 1.0021$$

TABLE B-8. $\Phi_{22/22}$ SPECTRA FOR Ω_{1N} = 225.0

Ω_1	Φ'	Φ	Φ'/Φ
.1000E-05	.1635E-01	.1626E-01	1.006
1.0000E-02	.1635E-01	.1626E-01	1.006
.2000E-01	.1635E-01	.1626E-01	1.006
.3000E-01	.1635E-01	.1626E-01	1.006
.4000E-01	.1635E-01	.1626E-01	1.006
.5000E-01	.1635E-01	.1626E-01	1.006
.6000E-01	.1635E-01	.1626E-01	1.006
.7000E-01	.1635E-01	.1626E-01	1.006
.8000E-01	.1635E-01	.1626E-01	1.006
.9000E-01	.1636E-01	.1626E-01	1.006
1.0000E-01	.1636E-01	.1627E-01	1.006
.1900	.1638E-01	.1629E-01	1.006
.2800	.1642E-01	.1632E-01	1.006
.3700	.1646E-01	.1637E-01	1.006
.4600	.1650E-01	.1641E-01	1.006
.5500	.1655E-01	.1646E-01	1.006
.6400	.1660E-01	.1650E-01	1.006
.7300	.1663E-01	.1654E-01	1.006
.8200	.1667E-01	.1657E-01	1.006
.9100	.1670E-01	.1660E-01	1.006
1.000	.1672E-01	.1662E-01	1.006
1.900	.1663E-01	.1653E-01	1.006
2.800	.1629E-01	.1619E-01	1.006
3.700	.1592E-01	.1582E-01	1.006
4.600	.1555E-01	.1545E-01	1.006
5.500	.1520E-01	.1510E-01	1.006
6.400	.1487E-01	.1477E-01	1.006
7.300	.1455E-01	.1447E-01	1.006
8.200	.1426E-01	.1418E-01	1.006
9.100	.1399E-01	.1391E-01	1.006
10.000	.1372E-01	.1365E-01	1.005
19.00	.1159E-01	.1161E-01	.9982
28.00	.9862E-02	.9995E-02	.9867
37.00	.8379E-02	.8603E-02	.9740
46.00	.7121E-02	.7385E-02	.9642
55.00	.6087E-02	.6322E-02	.9629
64.00	.5276E-02	.5402E-02	.9766
73.00	.4681E-02	.4613E-02	1.015
82.00	.4425E-02	.3942E-02	1.123
86.30	.4409E-02	.3670E-02	1.201

$$\frac{\int_0^{\Omega_{1max}} \Phi'(\Omega_1)\,d\Omega_1}{\int_0^{\Omega_{1max}} \Phi(\Omega_1)\,d\Omega_1} = \frac{.71065}{.71615} = .99232$$

TABLE B-9. $\Phi_{22/33}$ SPECTRA FOR Ω_{1N} = 215.0

Ω_1	Φ'	Φ	Φ'/Φ
.1000E-05	.1441E-01	.1433E-01	1.006
1.0000E-02	.1441E-01	.1433E-01	1.006
.2000E-01	.1441E-01	.1433E-01	1.006
.3000E-01	.1441E-01	.1433E-01	1.006
.4000E-01	.1441E-01	.1433E-01	1.006
.5000E-01	.1441E-01	.1433E-01	1.006
.6000E-01	.1441E-01	.1433E-01	1.006
.7000E-01	.1441E-01	.1433E-01	1.006
.8000E-01	.1441E-01	.1433E-01	1.006
.9000E-01	.1441E-01	.1433E-01	1.006
1.0000E-01	.1441E-01	.1433E-01	1.006
.1900	.1441E-01	.1432E-01	1.006
.2800	.1440E-01	.1431E-01	1.006
.3700	.1438E-01	.1430E-01	1.006
.4600	.1437E-01	.1428E-01	1.006
.5500	.1435E-01	.1426E-01	1.006
.6400	.1432E-01	.1423E-01	1.006
.7300	.1429E-01	.1420E-01	1.006
.8200	.1426E-01	.1417E-01	1.006
.9100	.1422E-01	.1413E-01	1.006
1.000	.1419E-01	.1410E-01	1.006
1.900	.1373E-01	.1364E-01	1.007
2.800	.1327E-01	.1318E-01	1.007
3.700	.1286E-01	.1276E-01	1.008
4.600	.1248E-01	.1239E-01	1.008
5.500	.1215E-01	.1205E-01	1.008
6.400	.1184E-01	.1175E-01	1.008
7.300	.1156E-01	.1147E-01	1.008
8.200	.1130E-01	.1121E-01	1.008
9.100	.1106E-01	.1098E-01	1.008
10.000	.1083E-01	.1075E-01	1.007
19.00	.9047E-02	.9031E-02	1.002
28.00	.7741E-02	.7809E-02	.9921
37.00	.6723E-02	.6849E-02	.9816
46.00	.5902E-02	.6059E-02	.9741
55.00	.5252E-02	.5392E-02	.9739
64.00	.4752E-02	.4819E-02	.9862
73.00	.4393E-02	.4321E-02	1.017
82.00	.4236E-02	.3886E-02	1.090
86.30	.4224E-02	.3703E-02	1.141

$$\frac{\int_0^{\Omega_{1max}} \Phi'(\Omega_1)\,d\Omega_1}{\int_0^{\Omega_{1max}} \Phi(\Omega_1)\,d\Omega_1} = \frac{.58540}{.58704} = .99720$$

TABLE B-10. $\Phi_{33/11}$ SPECTRA FOR Ω_{1N} = 195.0

Ω_1	Φ'	Φ	Φ'/Φ
.1000E-05	.2198E-04	.2302E-11	.9549E+07
1.0000E-02	.2203E-04	.2302E-07	956.9
.2000E-01	.2212E-04	.9210E-07	240.1
.3000E-01	.2225E-04	.2073E-06	107.3
.4000E-01	.2244E-04	.3688E-06	60.85
.5000E-01	.2267E-04	.5766E-06	39.31
.6000E-01	.2294E-04	.8311E-06	27.61
.7000E-01	.2327E-04	.1132E-05	20.55
.8000E-01	.2364E-04	.1481E-05	15.96
.9000E-01	.2406E-04	.1877E-05	12.82
1.0000E-01	.2452E-04	.2321E-05	10.57
.1900	.3094E-04	.8542E-05	3.623
.2800	.4163E-04	.1903E-04	2.188
.3700	.5688E-04	.3407E-04	1.669
.4600	.7675E-04	.5374E-04	1.428
.5500	.1010E-03	.7776E-04	1.299
.6400	.1289E-03	.1055E-03	1.222
.7300	.1599E-03	.1363E-03	1.173
.8200	.1929E-03	.1691E-03	1.141
.9100	.2272E-03	.2032E-03	1.118
1.000	.2620E-03	.2377E-03	1.102
1.900	.5636E-03	.5374E-03	1.049
2.800	.7586E-03	.7304E-03	1.039
3.700	.8920E-03	.8619E-03	1.035
4.600	.9925E-03	.9607E-03	1.033
5.500	.1074E-02	.1040E-02	1.032
6.400	.1142E-02	.1107E-02	1.032
7.300	.1200E-02	.1164E-02	1.031
8.200	.1251E-02	.1214E-02	1.031
9.100	.1297E-02	.1258E-02	1.031
10.000	.1338E-02	.1298E-02	1.031
19.00	.1606E-02	.1564E-02	1.027
28.00	.1748E-02	.1717E-02	1.018
37.00	.1814E-02	.1803E-02	1.006
46.00	.1832E-02	.1844E-02	.9935
55.00	.1822E-02	.1854E-02	.9829
64.00	.1802E-02	.1843E-02	.9773
73.00	.1781E-02	.1818E-02	.9794
82.00	.1769E-02	.1784E-02	.9917
86.30	.1768E-02	.1765E-02	1.001

$$\frac{\int_0^{\Omega_{1max}} \Phi'(\Omega_1)d\Omega_1}{\int_0^{\Omega_{1max}} \Phi(\Omega_1)d\Omega_1} = \frac{.13500}{.13493} = 1.0006$$

TABLE B-11. $\Phi_{33/22}$ SPECTRA FOR Ω_{1N} = 245.0

Ω_1	Φ'	Φ	Φ'/Φ
.1000E-05	.3033E-01	.3023E-01	1.003
1.0000E-02	.3033E-01	.3023E-01	1.003
.2000E-01	.3033E-01	.3023E-01	1.003
.3000E-01	.3033E-01	.3023E-01	1.003
.4000E-01	.3033E-01	.3023E-01	1.003
.5000E-01	.3032E-01	.3022E-01	1.003
.6000E-01	.3032E-01	.3022E-01	1.003
.7000E-01	.3032E-01	.3022E-01	1.003
.8000E-01	.3032E-01	.3022E-01	1.003
.9000E-01	.3032E-01	.3022E-01	1.003
1.0000E-01	.3032E-01	.3022E-01	1.003
.1900	.3030E-01	.3020E-01	1.003
.2800	.3027E-01	.3017E-01	1.003
.3700	.3023E-01	.3013E-01	1.003
.4600	.3018E-01	.3008E-01	1.003
.5500	.3011E-01	.3001E-01	1.003
.6400	.3003E-01	.2993E-01	1.003
.7300	.2994E-01	.2984E-01	1.003
.8200	.2984E-01	.2974E-01	1.003
.9100	.2973E-01	.2962E-01	1.003
1.000	.2961E-01	.2950E-01	1.003
1.900	.2818E-01	.2808E-01	1.004
2.800	.2675E-01	.2665E-01	1.004
3.700	.2546E-01	.2536E-01	1.004
4.600	.2431E-01	.2421E-01	1.004
5.500	.2327E-01	.2318E-01	1.004
6.400	.2233E-01	.2224E-01	1.004
7.300	.2147E-01	.2139E-01	1.004
8.200	.2068E-01	.2060E-01	1.004
9.100	.1994E-01	.1987E-01	1.003
10.000	.1925E-01	.1919E-01	1.003
19.00	.1407E-01	.1411E-01	.9970
28.00	.1065E-01	.1077E-01	.9882
37.00	.8215E-02	.8384E-02	.9799
46.00	.6455E-02	.6611E-02	.9764
55.00	.5185E-02	.5271E-02	.9837
64.00	.4284E-02	.4246E-02	1.009
73.00	.3668E-02	.3454E-02	1.062
82.00	.3412E-02	.2836E-02	1.203
86.30	.3400E-02	2604E-02	1.306

$$\frac{\int_0^{\Omega_{1max}} \Phi'(\Omega_1)\,d\Omega_1}{\int_0^{\Omega_{1max}} \Phi(\Omega_1)\,d\Omega_1} = \frac{.81316}{.81281} = 1.0004$$

TABLE B-12. $\Phi_{33/33}$ SPECTRA FOR Ω_{1N} = 210.0

Ω_1	Φ'	Φ	Φ'/Φ
.1000E-05	.9120E-02	.9037E-02	1.009
1.0000E-02	.9120E-02	.9037E-02	1.009
.2000E-01	.9120E-02	.9037E-02	1.009
.3000E-01	.9120E-02	.9037E-02	1.009
.4000E-01	.9121E-02	.9038E-02	1.009
.5000E-01	.9121E-02	.9039E-02	1.009
.6000E-01	.9121E-02	.9039E-02	1.009
.7000E-01	.9122E-02	.9040E-02	1.009
.8000E-01	.9123E-02	.9040E-02	1.009
.9000E-01	.9124E-02	.9041E-02	1.009
1.0000E-01	.9125E-02	.9042E-02	1.009
1900	.9139E-02	.9055E-02	1.009
.2800	.9158E-02	.9074E-02	1.009
.3700	.9182E-02	.9098E-02	1.009
.4600	.9208E-02	.9123E-02	1.009
.5500	.9235E-02	.9149E-02	1.009
.6400	.9259E-02	.9174E-02	1.009
.7300	.9281E-02	.9195E-02	1.009
8200	.9301E-02	.9214E-02	1.009
.9100	.9316E-02	.9229E-02	1.009
1.000	.9327E-02	.9240E-02	1.009
1.900	.9282E-02	.9192E-02	1.010
2.800	.9103E-02	.9009E-02	1.010
3.700	.8899E-02	.8803E-02	1.011
4.600	.8699E-02	.8602E-02	1.011
5.500	.8509E-02	.8411E-02	1.012
6.400	.8331E-02	.8233E-02	1.012
7.300	.8164E-02	.8066E-02	1.012
8.200	.8008E-02	.7911E-02	1.012
9.100	.7862E-02	.7766E-02	1.012
10.000	.7726E-02	.7632E-02	1.012
19.00	.6693E-02	.6631E-02	1.009
28.00	.5929E-02	.5914E-02	1.003
37.00	.5321E-02	.5347E-02	.9951
46.00	.4833E-02	.4882E-02	.9900
55.00	.4447E-02	.4488E-02	.9909
64.00	.4152E-02	.4147E-02	1.001
73.00	.3943E-02	.3848E-02	1.025
82.00	.3850E-02	.3581E-02	1.075
86.30	.3842E-02	.3466E-02	1.108

$$\frac{\int_0^{\Omega_{1max}} \Phi'(\Omega_1)d\Omega_1}{\int_0^{\Omega_{1max}} \Phi(\Omega_1)d\Omega_1} = \frac{.45515}{.45221} = 1.0065$$

APPENDIX C

INVERSE FOURIER TRANSFORMS
OF THE
SQUARE ROOT OF THE GUST AND GUST GRADIENT SPECTRA

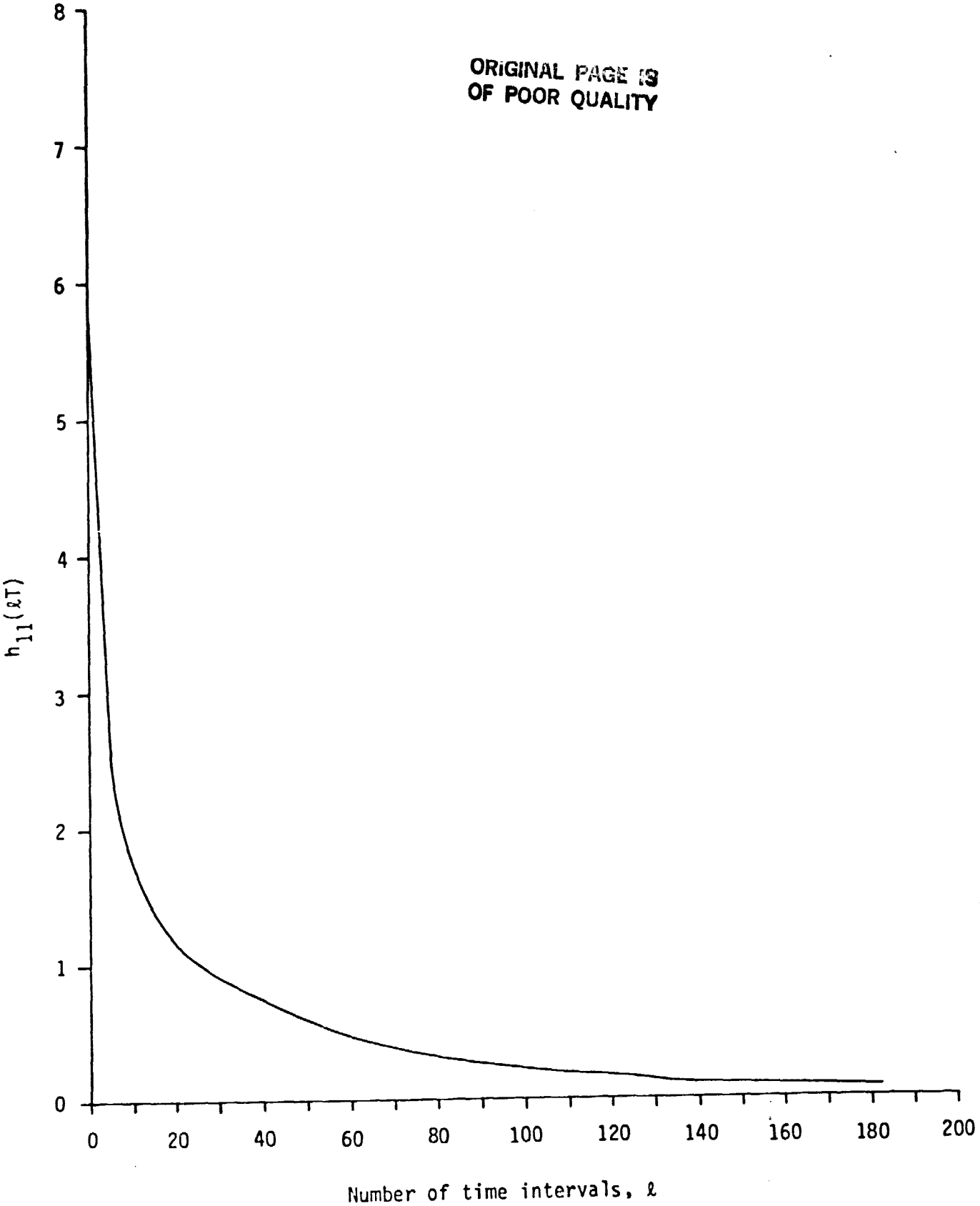

Figure C-1. Inverse Fourier Transform of $\sqrt{\Phi_{11}}$

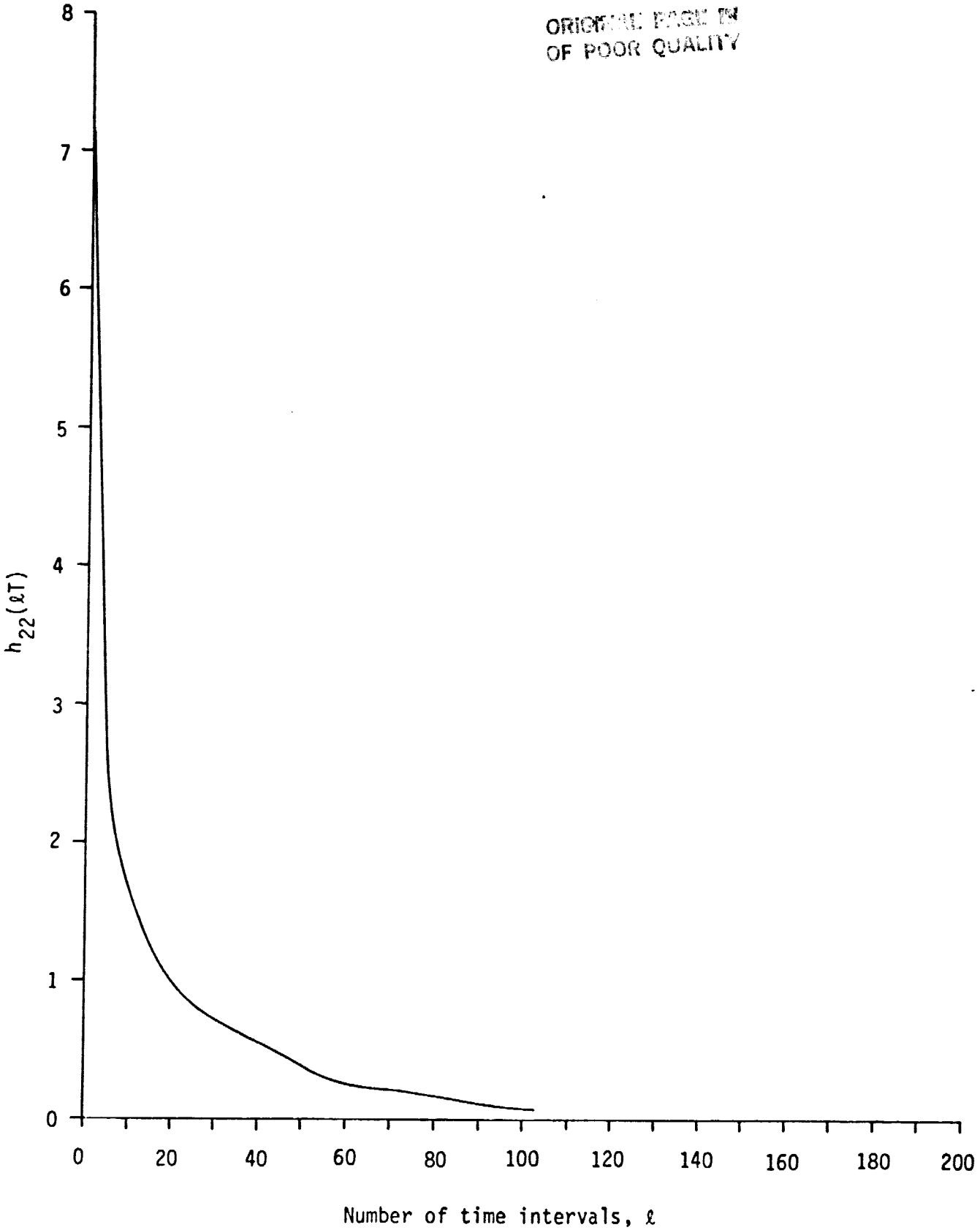

Figure C-2. Inverse Fourier Transform of $\sqrt{\Phi_{22}}$

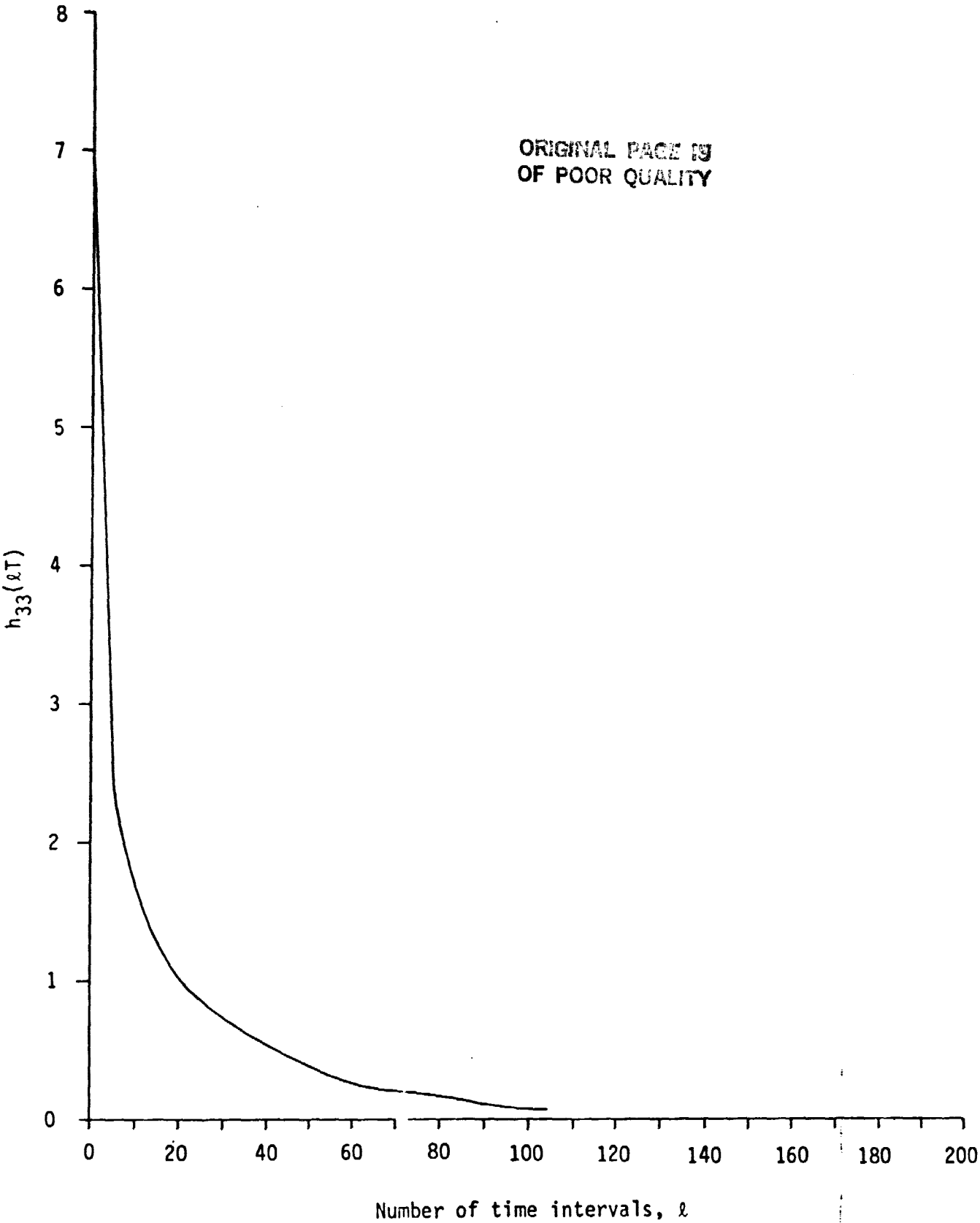

Figure C-3. Inverse Fourier Transform of $\sqrt{\Phi_{33}}$

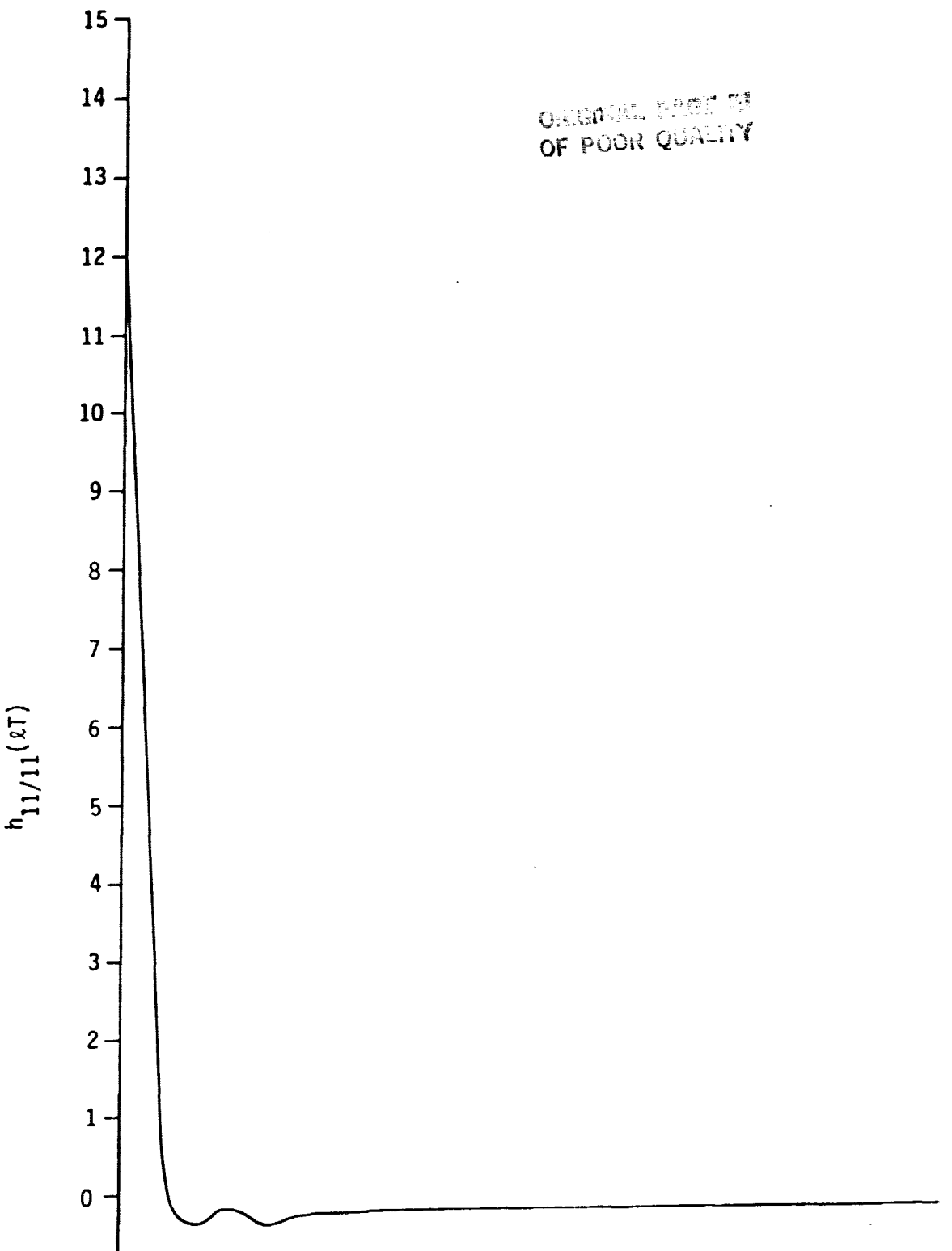

Figure C-4. Inverse Fourier Transform of $\sqrt{\Phi_{11/11}}$

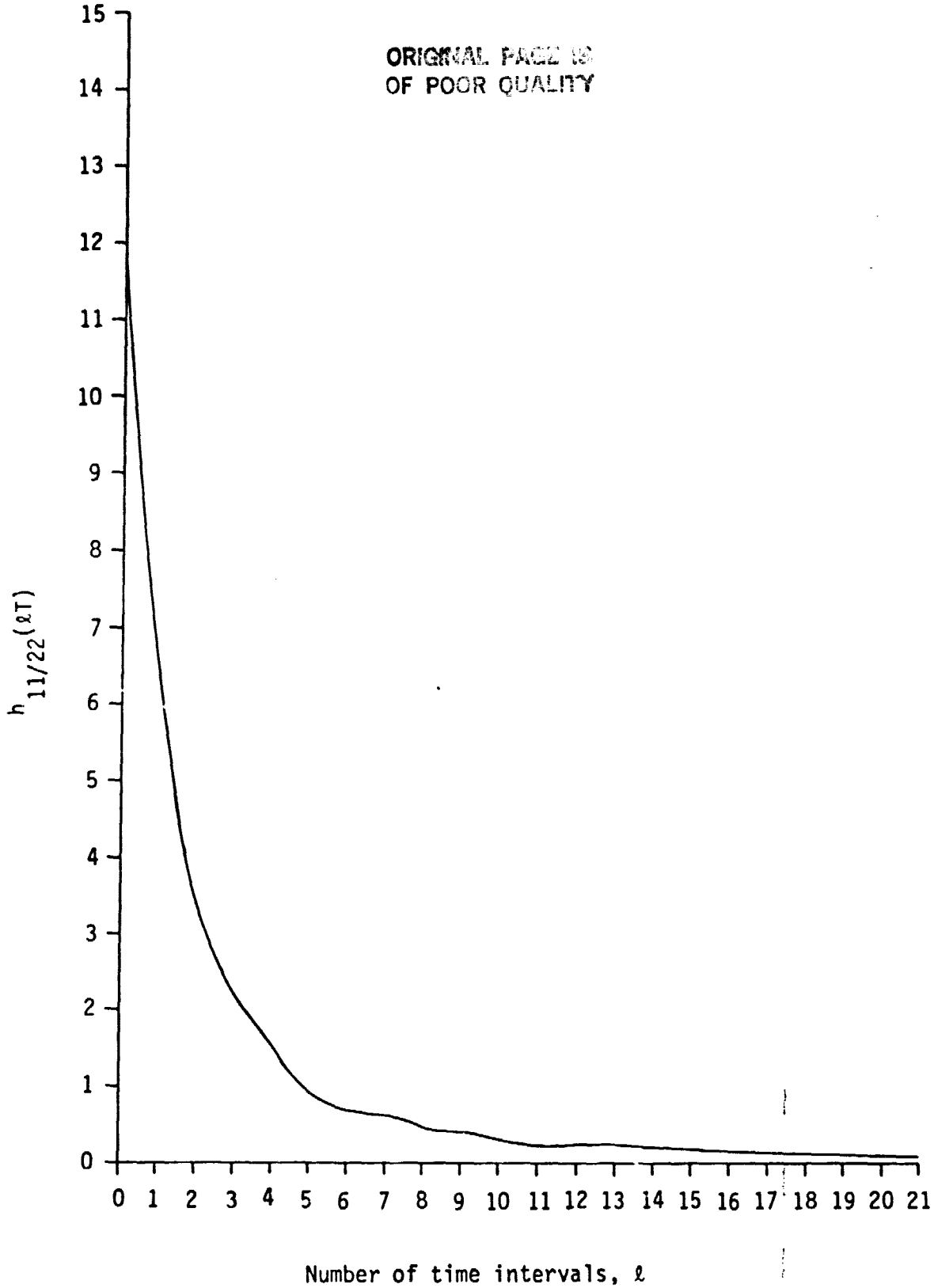

Figure C-5. Inverse Fourier Transform of $\sqrt{\Phi_{11/22}}$

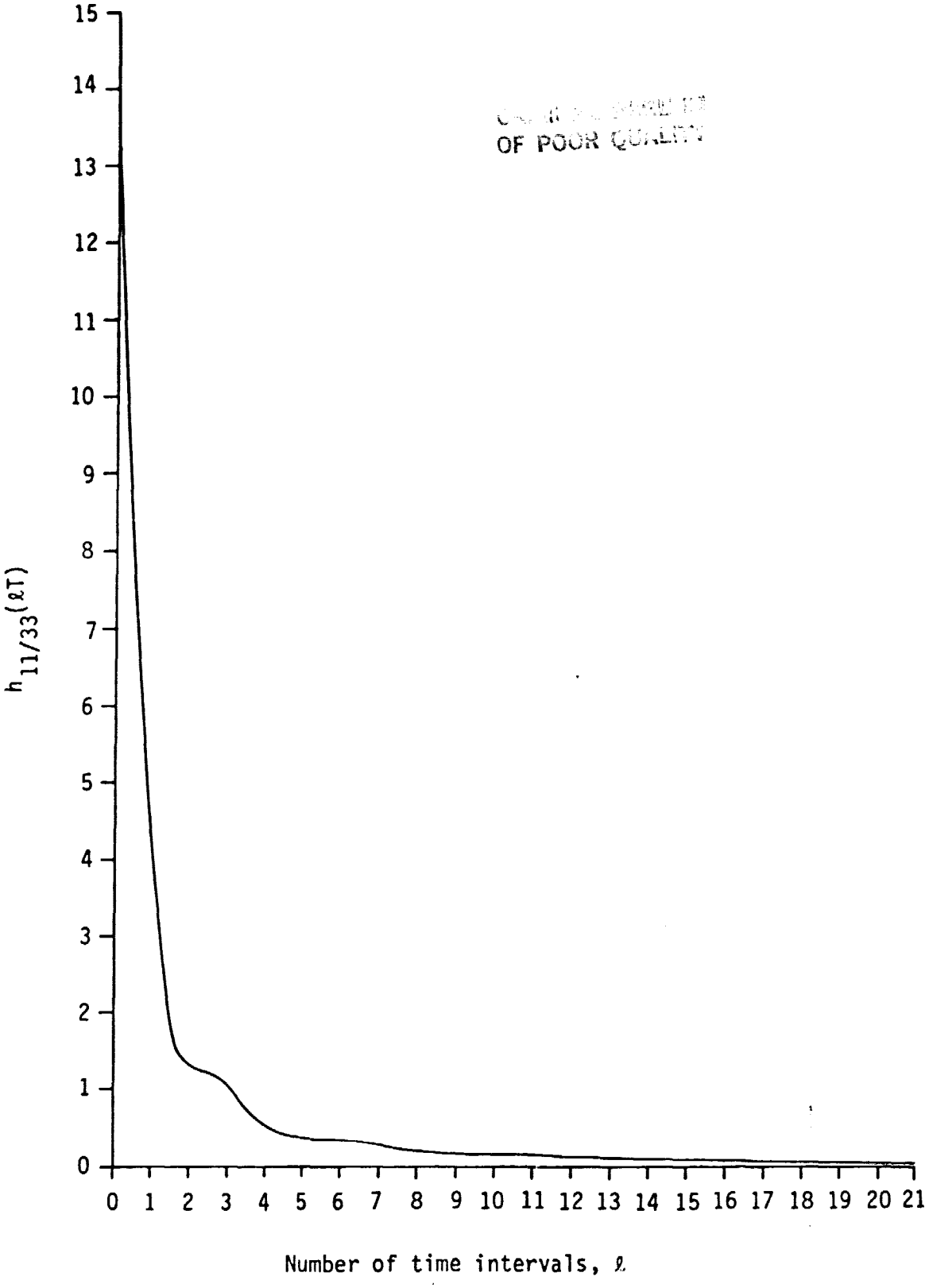

Figure C-6. Inverse Fourier Transform of $\sqrt{\Phi_{11/33}}$

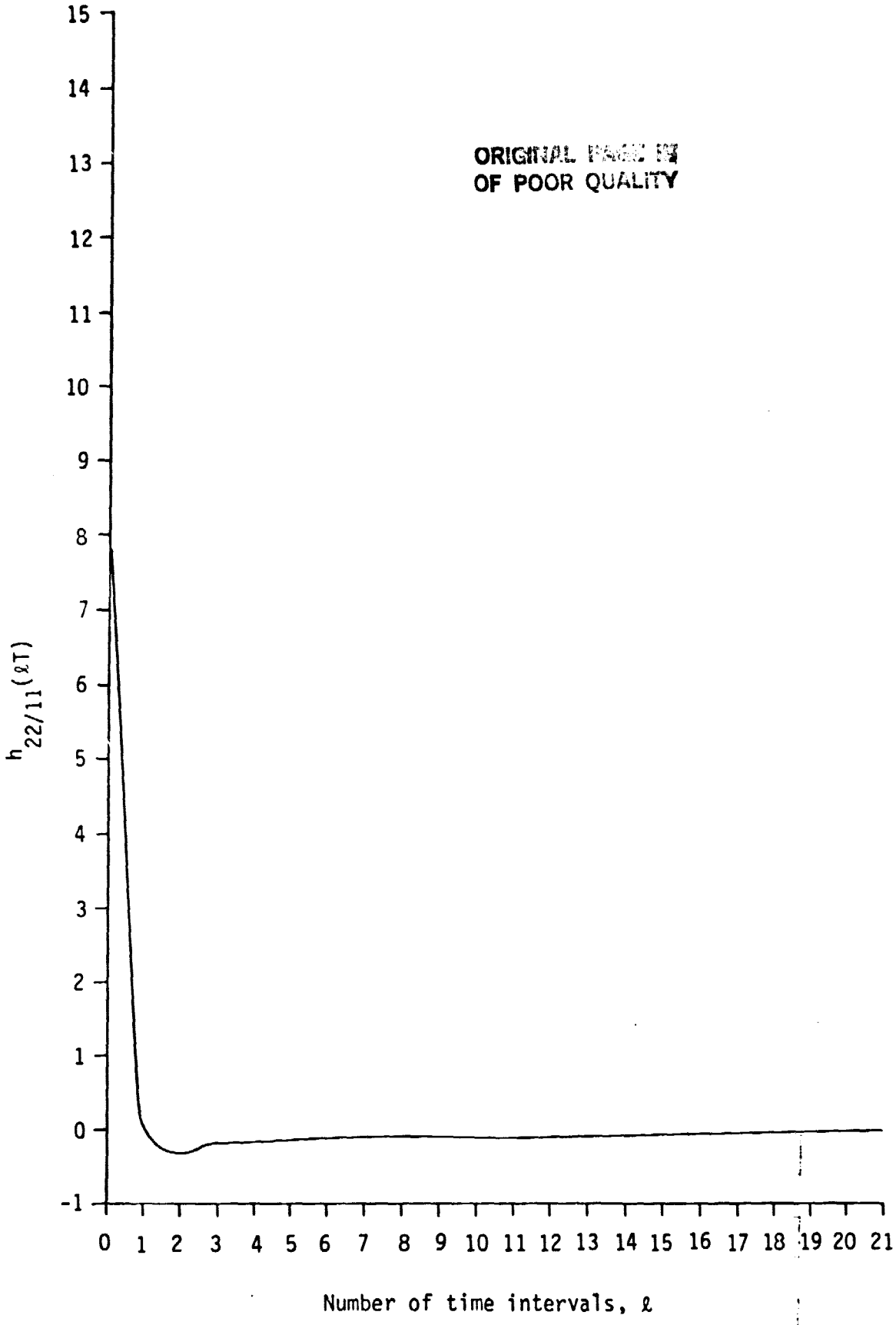

Figure C-7. Inverse Fourier Transform of $\sqrt{\Phi_{22/11}}$

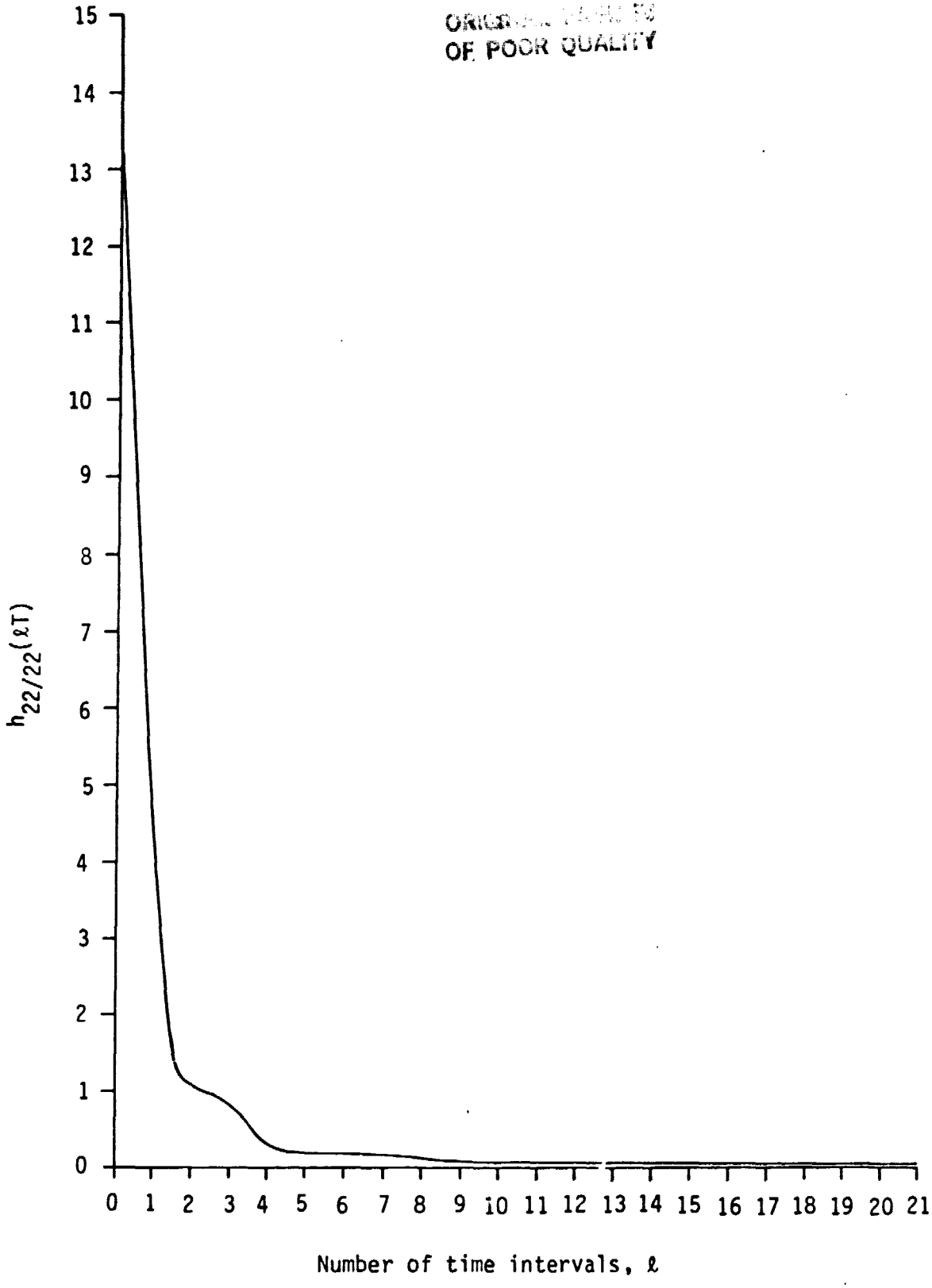

Figure C-8. Inverse Fourier Transform of $\sqrt{\Phi_{22/22}}$

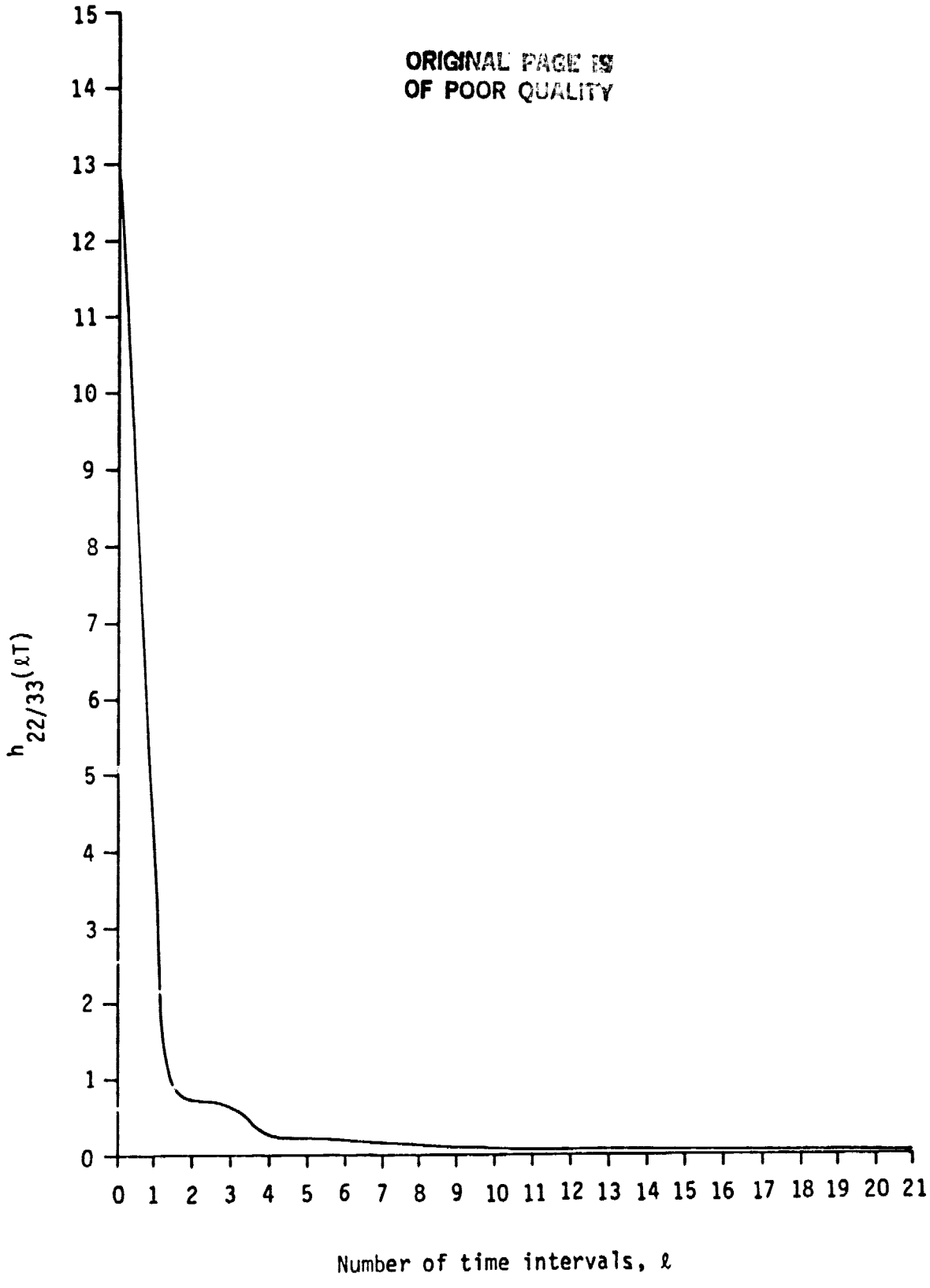

Figure C-9. Inverse Fourier Transform of $\sqrt{\Phi_{22/33}}$

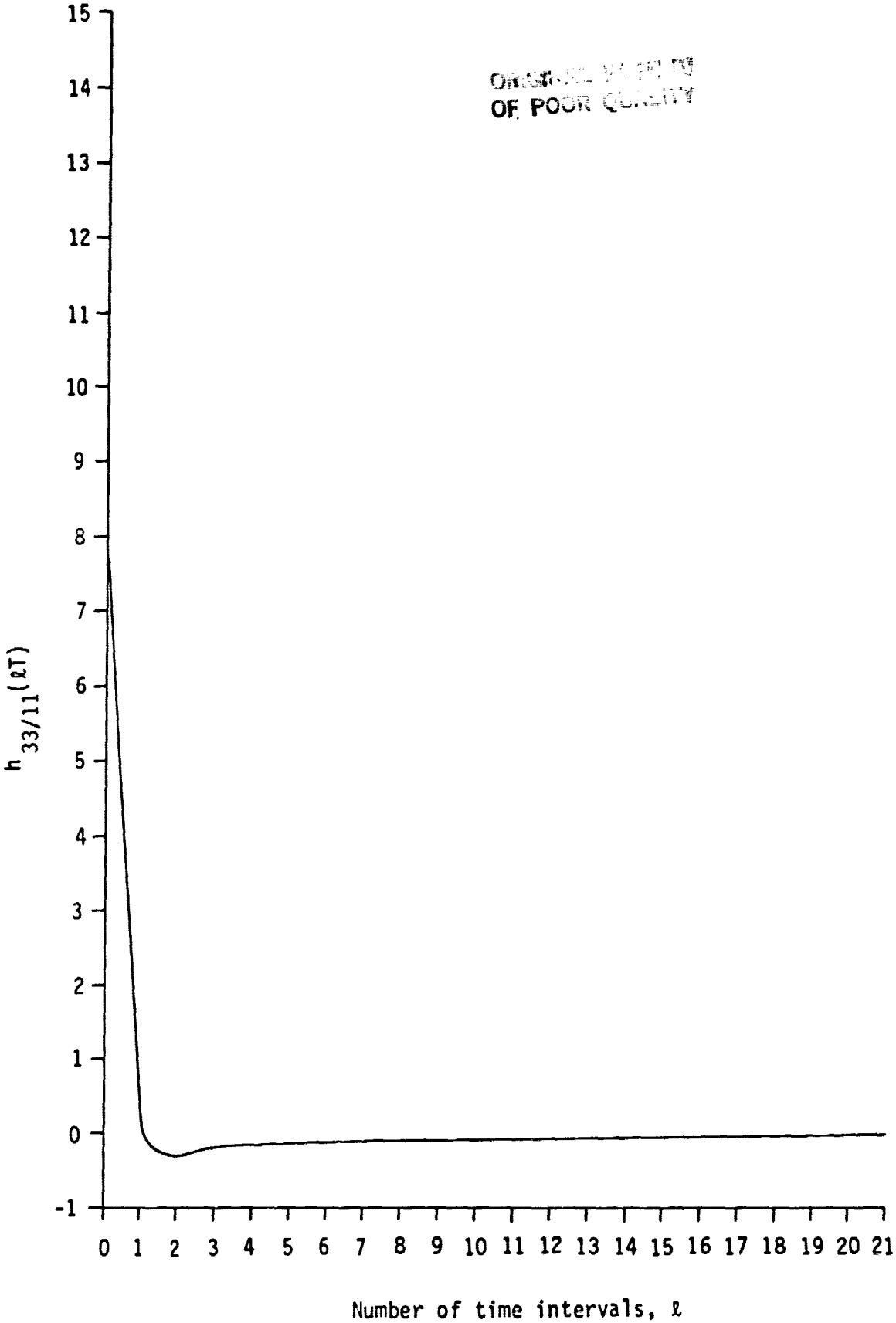

Figure C-10. Inverse Fourier Transform of $\sqrt{\Phi_{33/11}}$

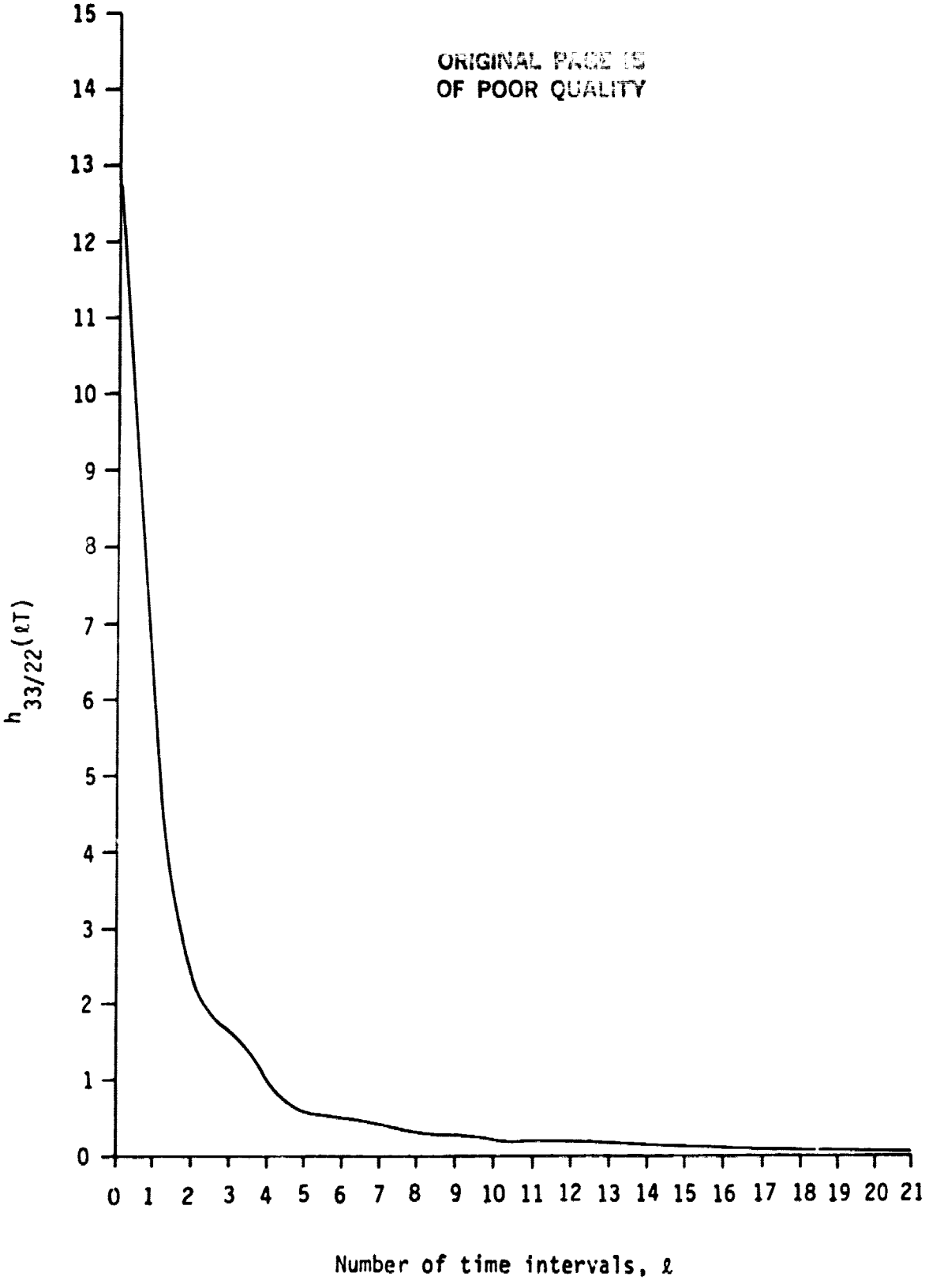

Figure C-11. Inverse Fourier Transform of $\sqrt{\Phi_{33/22}}$

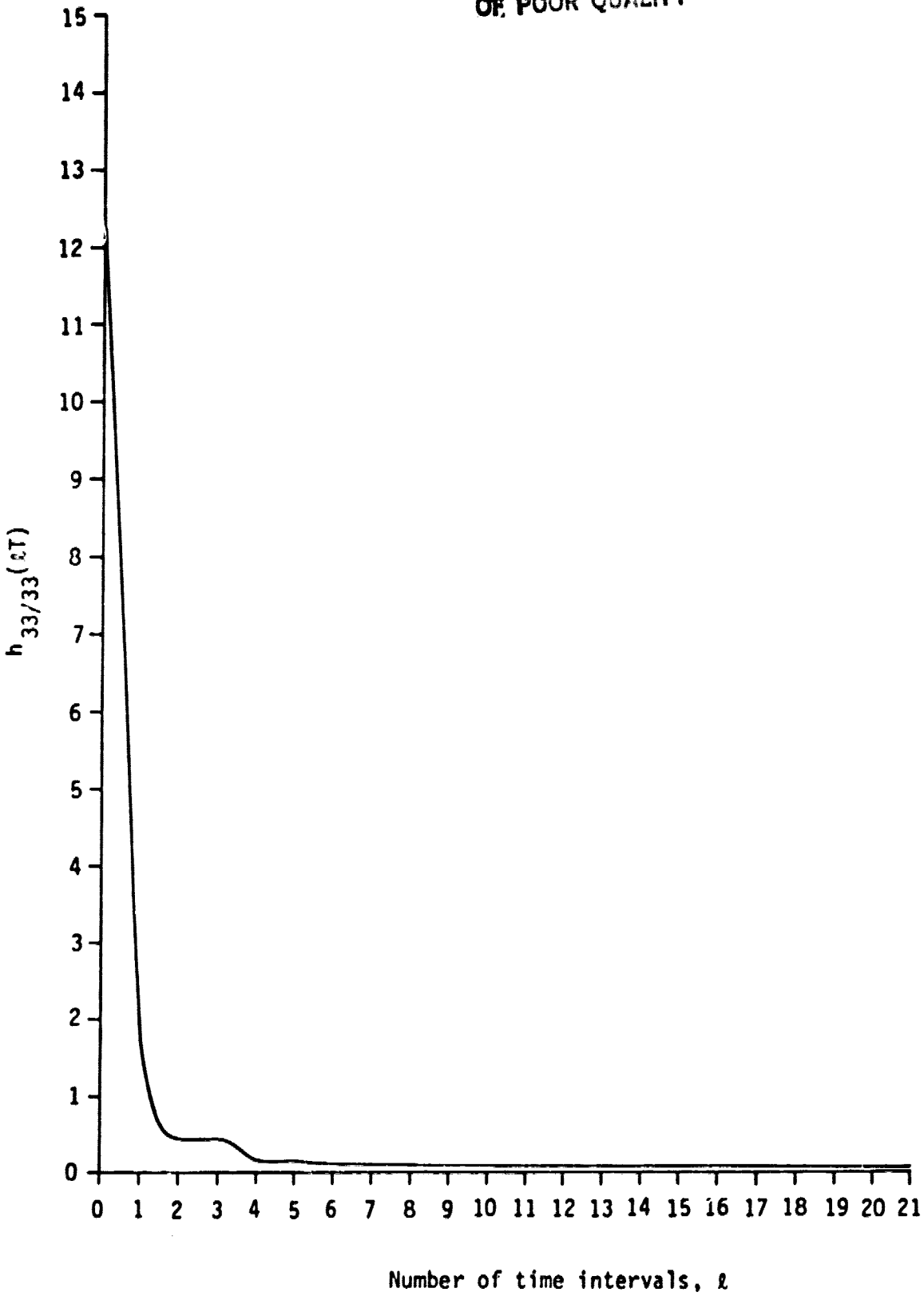

Figure C-12. Inverse Fourier Transform of $\sqrt{\Phi_{33/33}}$